A&A 592, A74 (2016)
DOI: 10.1051/0004-6361/201628241

Astronomy & Astrophysics

Highly variable AGN from the *XMM-Newton* slew survey

N. L. Strotjohann[1,2,3,4], R. D. Saxton[1], R. L. C. Starling[2], P. Esquej[5], A. M. Read[2], P. A. Evans[2], and G. Miniutti[6]

[1] XMM SOC, ESAC, Apartado 78, 28691 Villanueva de la Cañada, Madrid, Spain
[2] Dept. of Physics and Astronomy, University of Leicester, University Road, Leicester LE1 7RH, UK
[3] Physikalisches Institut, Universität Bonn, Nußallee 12, 53115 Bonn, Germany
[4] DESY, Platanenallee 6, 15738 Zeuthen, Germany
e-mail: nora.linn.strotjohann@desy.de
[5] Centro de Astrobiología (CSIC-INTA), 28850 Torrejón de Ardoz, Madrid, Spain
[6] Centro de Astrobiología (CSIC-INTA), Dep de Astrofísica; LAEFF, PO Box 78, 28691 Villanueva de la Cañada, Madrid, Spain

Received 3 February 2016 / Accepted 7 May 2016

ABSTRACT

Aims. We investigate the properties of a variability-selected complete sample of active galactic nuclei (AGN) in order to identify the mechanisms which cause large amplitude X-ray variability on timescales of years.
Methods. A complete sample of 24 sources was constructed, from AGN which changed their soft X-ray luminosity by more than one order of magnitude over 5–20 years between ROSAT observations and the *XMM-Newton* slew survey. Follow-up observations were obtained with the *Swift* satellite. We analysed the spectra of these AGN at the *Swift* and XMM observation epochs, where six sources had continued to display extreme variability. Multiwavelength data are used to calculate black hole masses and the relative X-ray brightness $\alpha_{\rm OX}$.
Results. After removal of two probable spurious sources, we find that the sample has global properties which differ little from a non-varying control sample drawn from the wider XMM-slew/ROSAT/Veron sample of all secure AGN detections. A wide range of AGN types are represented in the varying sample. The black hole mass distributions for the varying and non-varying sample are not significantly different. This suggests that long timescale variability is not strongly affected by black hole mass. There is marginal evidence that the variable sources have a lower redshift (2σ) and X-ray luminosity (1.7σ). Apart from two radio-loud sources, the sample sources have normal optical-X-ray ratios ($\alpha_{\rm OX}$) when at their peak but are X-ray weak during their lowest flux measurements.
Conclusions. Drawing on our results and other studies, we are able to identify a variety of variability mechanisms at play: tidal disruption events, jet activity, changes in absorption, thermal emission from the inner accretion disc, and variable accretion disc reflection. Little evidence for strong absorption is seen in the majority of the sample and single-component absorption can be excluded as the mechanism for most sources.

Key words. X-rays: general – galaxies: active – galaxies: Seyfert – quasars: general

1. Introduction

The X-ray emission of active galactic nuclei (AGN) probably arises from close to the central engine, and can display large amplitude variability on timescales of hours down to minutes. This variability is thought to be related to instabilities in the corona where UV photons are scattered to X-ray energies (Nandra 2001). Luminosity changes on longer timescales can be caused by perturbations in the accretion flow. This idea is supported by the correlation between luminosity, and thereby black hole mass and accretion rate, and variability timescale (e.g. McHardy et al. 2004, 2006), and by the observation of similar, lower amplitude variability observed in the optical and UV bands (e.g. MacLeod et al. 2010). A number of components can contribute to the X-ray spectrum of an AGN, and methods such as principle component analysis have identified a number of components contributing to variability across AGN samples on kilosecond (ks) timescales (Parker et al. 2015). These have been suggested to include relativistic reflection and changes in partial covering neutral absorption. On longer timescales of months to years, less is known about the X-ray variability mechanisms of AGN. A number of studies have probed the long-term light curves of samples at energies ≥2 keV (e.g. Sobolewska & Papadakis 2009; Winter et al. 2009; Soldi et al. 2014, using data from RXTE and *Swift* BAT). They successfully model this with changes in the flux and shape of the intrinsic power law emission. Extending this analysis down to soft X-ray energies, where disc, Compton and absorber contributions may play a significant role, requires data collection over multiple missions to cover long baselines in both time and energy range. This can be achieved with the AGN samples probed by the ROSAT all-sky survey (RASS; Voges et al. 1999) and the *XMM-Newton* slew survey (XMMSL1; Saxton et al. 2008). These X-ray surveys, taken about a decade apart, reach similar depths in the 0.2–2 keV band. Detailed studies have been carried out for a small number of individual objects demonstrating extreme X-ray variability. By way of an example, WPVS 007 showed a factor of 400 decrease in its soft X-ray flux between 1990 and 1993 (Grupe et al. 1995), the X-ray flux of PHL 1094 fell by a factor 260 over five years (Miniutti et al. 2012) and IRAS 13224-3809 has shown variations of a factor 50 on timescales of days (Boller et al. 1997). For individual objects significant advances in our understanding of variability mechanisms has been possible, but there remains a need both to characterise the highly X-ray variable AGN population and to identify the origins of these extreme flux changes. A change in absorbing column is among the proposed variability mechanisms at these energies and timescales. We know that cold and warm material is present in the broad- and narrow-line regions, and movement of clouds or outflowing material across the line-of-sight can dramatically

alter the observed soft X-ray spectral shape (e.g. Risaliti et al. 2005; Komossa & Fink 1997; Winter et al. 2012; Starling et al. 2014). The absorption seen in AGN is, in many cases, well described by clumpy, partial covering material which could feasibly provide year-timescale orbital variability. In Seyfert 2 galaxies in particular variability of clumpy X-ray absorbing material may be ubiquitous (Risaliti et al. 2002), while ionised absorbers may be common among luminous Seyfert 1s (Winter 2010). A statistical search for absorption events has been carried out on the long-term RXTE X-ray light curves of a sample of Seyfert galaxies, resulting in probability estimates for observing a source during an absorption event that echos the greater variability expectation for Seyfert 2s over Seyfert 1s (Markowitz et al. 2014). A steep flux increase which then decays may be indicative of a more catastrophic event such as a tidal disruption event (TDE, e.g. Rees 1988). Candidate TDEs have been found in ROSAT (Komossa & Bade 1999; Greiner et al. 2000) and XMM observations (Esquej et al. 2007; Saxton et al. 2012; Maksym et al. 2010) as well as at UV (e.g. Gezari et al. 2008; van Velzen et al. 2011) and optical wavelengths (e.g. Komossa et al. 2008; Arcavi et al. 2014; see Komossa 2015 for a review). Similarly to the likely origins of short timescale variability, intrinsic changes in accretion onto the black hole (Miniutti et al. 2013; Shappee et al. 2014; Saxton et al. 2014), as well as jet power and changes in the Comptonising media may be responsible. By observing both the soft and hard X-ray bands simultaneously, the interplay between the underlying emission and any absorption components may be derived. In this paper we examine a sample of candidate AGN drawn from the *XMM-Newton* slew survey which have shown large-amplitude long-timescale soft X-ray variability when compared with earlier ROSAT data. We re-observed these sources in a dedicated *Swift* programme, and combined these data with archival multiwavelength data in order both to identify the soft X-ray variability mechanisms in each individual source, and to characterise the highly variable AGN population. In Sect. 2 we describe the sample selection and compare our sample with a wider sample of AGN drawn from the XMM slew survey in Sect. 3. In Sect. 4 we present the *Swift* X-ray telescope (XRT) observations from our targeted programme and show the long-term light curves in Sect. 5. Optical to X-ray flux ratios are calculated in Sect. 6. We go on to look at the spectra obtained with *Swift* and XMM for our sample in Sect. 7, to understand the variability mechanisms which may be at play. Finally, we discuss our results in the context of long-term X-ray variability and highly variable AGN populations in Sect. 8. The results for each individual source are detailed in Appendix A. A λCDM cosmology with $(\Omega_{\rm M}, \Omega_{\lambda}) = (0.3, 0.7)$ and $H_0 = 70$ km^{-1} s^{-1} Mpc^{-1} has been assumed throughout.

2. Sample selection

The *XMM-Newton* slew survey (XMMSL1; Saxton et al. 2008), with positional accuracy of 8″ and soft flux sensitivity of $F_{0.2\text{-}2.0\,\rm keV} = 6 \times 10^{-13}$ erg cm^{-2} s^{-1}, has characteristics which are well matched with those of the ROSAT all-sky survey (RASS; Voges et al. 1999) performed at the beginning of the 1990s. This allows meaningful flux comparisons to be made of sources observed with both satellites. We consider all XMMSL1 sources, with counterparts identified as AGN or galaxies. The identification procedure is outlined in Saxton et al. (2008). AGN have principally been identified from SIMBAD, NED, SDSS, 2MASS extended sources and the Veron catalogue (Véron-Cetty & Véron 2006). From these AGN candidates we have selected a complete sample of sources which have varied by more than a factor of ten when comparing the 0.2–2 keV flux in the XMMSL1 observations to fluxes (or 2σ flux limits) seen in the RASS or in ROSAT pointed observations from 5–19 years earlier. Since some flux measurements have large associated uncertainties we calculate the 1σ error on the flux ratio and only select the source if the ratio is still larger than ten when considering the error. Variability in the harder part of the spectrum is not explored here, as no wide area 2–10 keV survey exists with comparable sensitivity to XMMSL1. The sample contains all objects that meet these criteria and that are included in the XMMSL1-Delta-3 catalogue which contains data from slews made between 2001-08-26 and 2009-01-15. To convert ROSAT and XMM count rates to fluxes, we have adopted a spectral model of an absorbed power law with a typical AGN photon index of $\Gamma = 1.7$ (Turner & Pounds 1989) and Galactic absorption per source according to Willingale et al. (2013). Inaccuracies introduced in the flux ratios by the use of this fixed spectral slope are discussed in Saxton et al. (2011). The flux ratio will also be affected if the source spectrum changes between the ROSAT and XMM slew observations; a point which is quantitatively addressed in Sect. 5. This resulted in 24 XMMSL1 sources, listed in Table 1, which form a complete sample selected on the basis of large amplitude soft X-ray variability. The slew survey is sensitive to relatively bright sources and many of the detected objects are nearby AGN. Two of our sample sources, ESO 362-G018 and 1H 0707-495, have been extensively discussed in the literature; here we summarise only the most relevant results. A further two sources, NGC 3599 and SDSS J132341.97+482701.2, have been identified as tidal disruption candidates in non-active, or weakly active, galaxies (see Esquej et al. 2007, 2008) and will only be peripherally discussed in this paper.

3. Comparison with the wider XMM slew survey AGN sample

In order to put our 24 candidate highly variable AGN into context, we examine the count rates of all secure AGN detected in the XMM slew survey. We have made a new selection consisting of all sources observed within XMMSL1-Delta-3 and ROSAT which are contained in the Veron catalogue of AGN (Véron-Cetty & Véron 2006). This produces a sample of 1038 AGN, discussed previously in Saxton et al. (2011), which we call here the Veron sample. For a source to be included in our sample of highly variable candidate AGN it must have observations with both ROSAT and XMM that are deep enough that strong variability, between the XMM and ROSAT flux or upper limit, can be detected. To be able to compare the Veron sample to the highly variable AGN candidates we remove all sources from the Veron sample for which such a high variability is not detectable. From the ROSAT catalogues for bright sources, faint sources and pointed observations, we obtain the exposure times, background rates and extraction radii. With this information we calculate the 90% noise level during the ROSAT observation. A source fainter by a factor of ten compared to the slew survey has a count rate reduced by a factor of 70, if observed with ROSAT (see Saxton et al. 2011) due to the smaller effective area. We only select the sources from the Veron sample for which this count rate would be above the noise level. This condition is fulfilled by 728 or 70% of the sources. Figure 1 shows that the sources removed are mainly those with low count rates during the slew survey. In Fig. 1 we subdivide the remaining AGN of the Veron sample by their flux ratio. The yellow line shows the population of 35 sources in the Veron sample which are at least ten times brighter during the slew survey. The sample

Table 1. High variability candidate AGN sample.

XMMSL1 name	Type	z	$L_{X,0.2-2\,keV}$ (10^{42} erg s^{-1})	XMM/RASS ratio	0.2–2 keV CR ct s^{-1}	2–10 keV CR ct s^{-1}	M_{bh} log($M_\odot$)	Common name
J005953.1+314934	Sy 1.2	0.0149	5.5	12.4 ± 1.4	8.14 ± 0.79	1.76 ± 0.39	6.5	Mrk 352
J015510.9-140028	–	–	–	>45.0	0.63 ± 0.27	–	–	
J020303.1-074154	Sy 1	0.0615	25.6	>38.4	2.15 ± 0.59	–	6.8	2MASX J02030314-0741514
J024916.6-041244	Sy 1.9	0.0186	1.9	>24.6	1.84 ± 0.80	–	5.7	2MASX J02491731-0412521
J034555.1-355959[a]	–	–	–	>15.3	1.06 ± 0.29	1.463 ± 0.384	–	MRSS 358-033707
J044347.0+285822[a]	Sy 1	0.0217	2.6	15.7 ± 4.2	1.62 ± 0.46	1.60 ± 0.58	7.3	UGC 3142
J045740.0-503053	–	–	–	>18.1	2.25 ± 0.48	–	–	2MASX J04574068-5030583
J051935.5-323928[a]	Sy 1.5	0.0125	0.76	18.0 ± 6.4	7.57 ± 0.97	1.021 ± 0.396	6.6	ESO 362-G018
J064541.1-590851[a]	–	–	–	>29.9	1.09 ± 0.35	0.785 ± 0.430	–	2MASX J06454155-5908456
J070841.3-493305[a]	NLS 1	0.0406	14.5	13.4 ± 2.2	6.63 ± 1.04	–	7.1	1H 0707-495
J082753.7+521800[a]	QSO	0.3378	578	>16.3	1.14 ± 0.24	0.629 ± 0.277	7.8	87GB 082409.1+522804
J090421.2+170927	QSO	0.0733	15.9	>32.5	0.91 ± 0.25	–	7.4	SDSS J090421.39+170933.2
J093922.5+370945	NLS 1	0.1861	241	>33.9	1.90 ± 0.39	–	7.9	2MASS J09392289+3709438
J100534.8+392856	Sy 1	0.1409	106	>15.4	1.55 ± 0.22	–	7.8	2MASX J10053467+3928530
J104745.6-375932	Sy 1	0.0755	47	>13.3	2.51 ± 0.39	–	7.2	6dFGS gJ104745.7-375932
J111527.3+180638	liner	0.00278	0.073	>54.4	4.95 ± 0.65	–	–	NGC 3599
J112841.5+575017[a]	Sy 2	0.0509	10.9	>17.8	1.37 ± 0.34	0.43 ± 0.18	7.6	MCG+10-17-004
J113001.8+020007	–	–	–	>21.0	1.47 ± 0.43	–	–	
J121335.0+325609	QSO	0.222	154	21.0 ± 7.3	0.82 ± 0.19	–	7.9	SDSS J121334.67+325615.2
J132342.3+482701	inactive	0.0875	39	>38.1	1.60 ± 0.37	–	–	SDSS J132341.97+482701.2
J162553.4+562735[a]	QSO	0.307	442	>26.4	1.11 ± 0.28	–	7.9	SBS 1624+565
J173739.3-595625[a]	Sy 2	0.0170	3.09	>19.4	4.20 ± 0.82	1.47 ± 0.40	7.3	ESO 139-G012
J183521.4+611942[a]	blazar	2.274	61 449	16.9 ± 6.7	1.16 ± 0.26	–	9.7	QSO J1835+6119
J193439.3+490922[a]	–	–	–	>26.1	0.95 ± 0.32	–	–	2MASX J19343950+4909211

Notes. Information on the AGN type, redshift and common name were obtained from the NASA/IPAC Extragalactic Database (NED; https://ned.ipac.caltech.edu/) and references therein. L_X is the luminosity as seen in the XMM slew survey in the 0.2–2.0 keV band, calculated using a model of a power of index $\Gamma = 1.7$ and Galactic absorption. The XMM/RASS ratio is the ratio of the XMM slew and ROSAT fluxes, or upper limits, for the 0.2–2 keV energy range, using the same spectral model. Errors are 1σ. The black hole masses have been estimated using the k-band luminosity as described in Sect. 3 and have a typical uncertainty of 0.3 dex. [(a)] Some sources have several slew survey observations. In those cases we list the first observation in which a significant flux change by at least a factor of ten was observed compared to the ROSAT flux, or upper limit, in the 0.2–2 keV band. The soft, 0.2–2 keV, and hard, 2–10 keV, count rates correspond to the values seen in this slew observation. The hard band count rate is only quoted if the source was actually detected in this band.

discussed in this paper (shown as a red dashed line) has a large overlap with the highly variable Veron AGN and the count rate distributions are similar. Some of our sources are, however, not contained in the Veron catalog. In addition we take into account the statistical errors on the count rates and only select sources with a flux ratio significantly above the threshold of ten. We then selected sources that were observed to vary only by a factor of $\leqslant 3$ and defined those as the constant sample. In Fig. 2 we show the redshift and X-ray luminosity of our highly variable sample overlaid on that of the constant sample. Projecting the distributions on the axes, one sees that our sample is slightly biased towards lower values for both quantities. An exception is XMMSL1 J183521.4+611942, known to be a bright blazar at $z = 2.2$. Using the Kolmogorov-Smirnov test we examine whether the variable sources are drawn randomly from the same sample as the constant sources. The probability that this is true for the redshift is 2.2%, while for the X-ray luminosity it is 2.6%. Among our highly variable sample we know we have two candidate TDEs, and if we omit these we obtain probabilities of 2.5% (redshift, deviation at 2σ level) and 4.6% (luminosity, deviation at 1.7σ level). In addition, neglecting the blazar, which is atypical of our candidate AGN sample, would increase the significance by 0.3σ for both distributions. We thus conclude that there are indications that highly variable sources tend to have lower X-ray luminosities than other AGN and are therefore only observed at lower redshifts. However this result is not statistically significant and larger samples would be necessary to confirm this. One other fundamental AGN property is the black hole mass. Unfortunately precise mass estimates obtained for example from stellar dynamics or reverberation mapping are not available for most AGN in our sample. We therefore have to rely on a more indirect and less precise approach. Here we use the empirical correlation between the k-band luminosity and the black hole mass as described in Marconi & Hunt (2003). The scatter of this method is 0.3 dex. Since all our sources are contained in the 2MASS catalogues, the black hole mass can be calculated in this way for all sources except for the six galaxies lacking a redshift measurement (Table 1). We also omit the two likely tidal disruption candidates. The k-band magnitudes are obtained from the NASA/IPAC Infrared Science Archive. If there is in addition an entry in the extended source catalogue, we use this value, which is only significantly larger for the closest sources. The k-magnitude has to be corrected for the contribution of the host galaxy to obtain the luminosity of the bulge alone (Simien & de Vaucouleurs 1986). However in most cases the type of the host galaxy is unknown, so for those galaxies we use a correction of 0.8 mag corresponding to a lenticular host galaxy, which is in between the correction for an elliptical and a spiral galaxy. The resulting mass estimates are given in Table 1. The black hole mass has also been estimated using other methods, including the optical Hβ line width or reverberation measurements, for seven of our sample sources

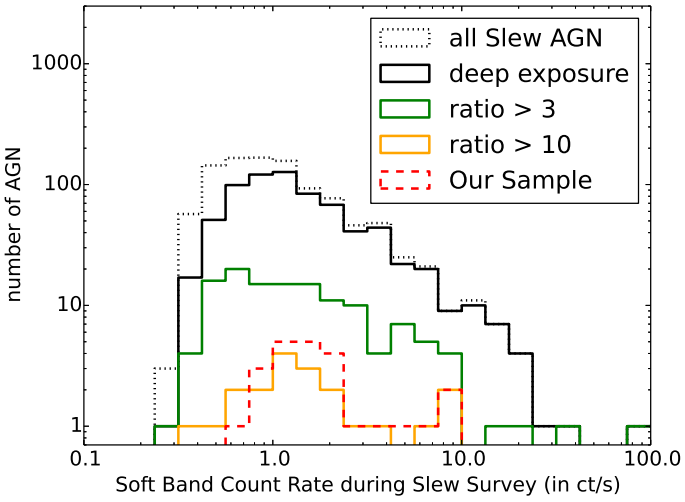

Fig. 1. Histogram of XMMSL1 soft-band count rates. The black dashed line shows all detected sources from the Veron sample (see text) while the black solid line corresponds to the fraction of the Veron sample with deep enough ROSAT observations, such that a factor of ten variability in flux between XMMSL1 and ROSAT would have been detected. The green and yellow lines represent sources that fulfil this criterion and that were also observed to vary by a factor of more than three or ten respectively. Our so-called constant sample consists of all sources in-between the black and the green line, while the variable sources are the ones below the red line. Some low-count sources contained within the yellow line have errors on their flux ratios which exclude them from the variable sample and the variable sample includes several AGN which are not in the Veron catalog.

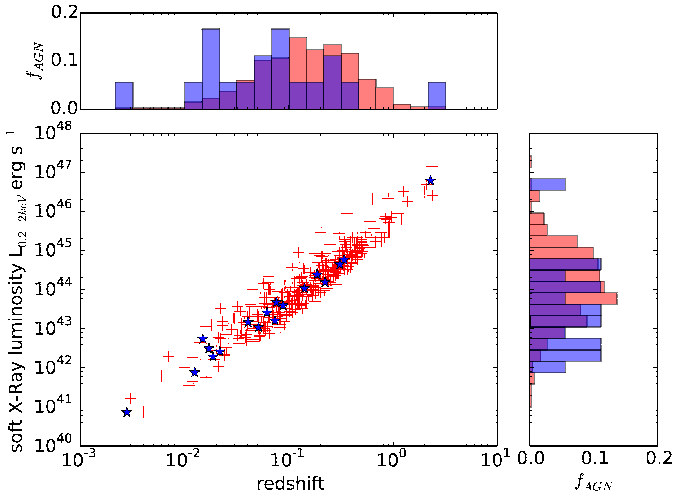

Fig. 2. Comparison between the constant and highly variable samples. In the main panel we plot the 0.2–2 keV luminosity during the XMM slew survey against redshift. Red crosses represent constant sources while the blue stars correspond to the highly variable sources. The subplots show the fraction of sources, $f_{\rm AGN}$, in the samples at each luminosity and redshift, where red bars show constant sources and blue bars variable sources.

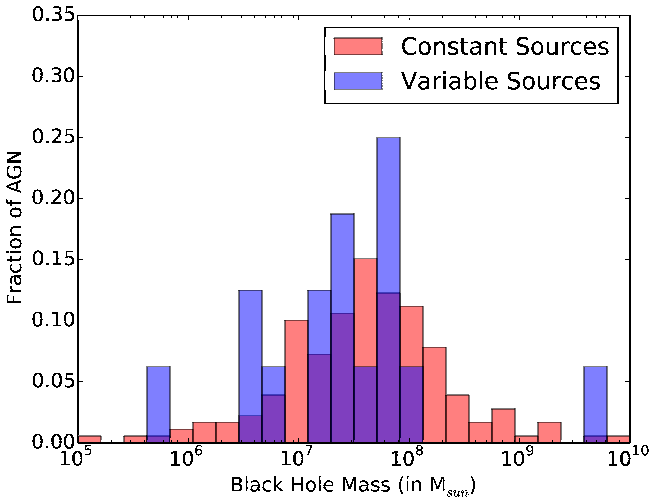

Fig. 3. The mass distribution from the *k*-band luminosity for the constant sample and for our variable AGN.

as reported in the literature (Greene & Ho 2007; Ho et al. 2008; Shen et al. 2008; Parisi et al. 2009; Caramete & Biermann 2010; Fabian et al. 2012; Ponti et al. 2012; Winter et al. 2012; Zhou & Soria 2013). For some sources we obtain an additional mass estimate using the excess variance method (O'Neill et al. 2005; Ponti et al. 2012). For most sources the mass estimates are consistent within an order of magnitude, highlighting that the masses presented here are not very precise and should be considered as order of magnitude estimates. In Fig. 3 we show the mass distribution of the highly variable sources compared to the masses of the constant sample. Since the variable sources are on average at lower redshifts as shown in Fig. 2, we would expect this to translate into lower black hole masses. There is a small difference between the two samples, however the probability that both distributions are drawn from the same sample is 32%. Thus we cannot reject this hypothesis. Maybe the effect may be diluted by the intrinsic scatter in the relation and the additional uncertainty introduced by not being able to correct for the individual host galaxies. Moreover we know that there are several variability mechanisms and some of them might correlate with the host mass, while others might not, or might even be anticorrelated. With our small sample we are not able to distinguish between individual populations of highly variable AGN, for example high mass blazars and low mass intrinsically variable AGN. We conclude that even though we might expect to see a bias towards lower black hole masses due to the lower redshifts and X-ray luminosities, we do not see any significant deviation.

4. *Swift* observations

We observed our full sample of all 24 candidate highly variable AGN with *Swift* (Gehrels et al. 2004) for ~2 ks each, between 2010 and 2014 as part of a fill-in programme. All XRT (Burrows et al. 2005) observations were made in photon counting mode with exposure times ranging from 1.6–3.7 ks. The *Swift*-XRT data were obtained from the UK *Swift* Science Data Centre[1] and reduced following the procedures of Evans et al. (2009) using the *Swift* software and calibration database available within HEASOFT v.6.12. Simultaneous observations were made with the *Swift* BAT (Barthelmy et al. 2005) at 14–195 keV and the *Swift* UV/Optical Telescope (UVOT; Roming et al. 2005) with the u filter applied. For ten sources, additional archival *Swift* observations were available at the time of writing which we have included and analysed in an identical manner. Details of all the observations used in this paper are given in the appendix (see Table A.1). With the XRT we detected 16 (or two-thirds) of the sample sources in our fill-in observations.

[1] www.swift.ac.uk/user_objects

Widening our search, we looked at data stacks in the *Swift* XRT Point Source Catalogue (1SXPS; Evans et al. 2014) and other pointed XRT observations and found that a further five sources were detected. Two of the three XRT non-detected sources have only ever been detected in the XMM slew survey (Figs. 1b and f), and cannot be identified with any source detected in other wavelength surveys such as 2MASS, WISE, SDSS or 6dF in our searches. One of these, XMMSL1 J015510.9-140028, lies at the detection threshold of the slew survey. The other, XMMSL1 J113001.8+020007, has a higher significance, however the photons at the source location are aligned along a row which indicates that this might not be an astrophysical point source. We conclude therefore that those two detections in the slew survey are highly likely to be spurious. We discuss the spurious fraction further in Sect. 8. The remaining XRT-undetected source is XMMSL1 J193439.3+490922, which has three detections in XMM slews and is hence likely real. All XRT-detected sources are also detected with UVOT. Three sources (Mrk 352, ESO 362-G018, ESO 139-G012) can be found in the *Swift* BAT 70-month All-Sky Hard X-ray Survey Source Catalog (Baumgartner et al. 2013).

5. Long-term X-ray light curves

In Fig. B.1 we plot the soft X-ray light curves for our candidate highly variable AGN using available X-ray data taken by the satellite missions *Einstein*, ROSAT, XMM, *Suzaku* and *Swift*. The count rates were obtained from different archives including HEASARC, the XMM Science Archive, the *Swift* UKSSDC and from our own *Swift* XRT data analysis, and for upper limits the 1SXPS catalogue (Evans et al. 2014) and the XMM upper limit server[2] were queried. The count rates of the different satellites were converted to fluxes between 0.2–2.0 keV using PIMMS[3] assuming a power law with a photon index of 1.7 as a spectral shape taking into account Galactic extinction as given by Willingale et al. (2013). Sobolewska & Papadakis (2009) found a positive correlation between flux and spectral slope for a sample of bright RXTE AGN in the 2–10 keV band. This could affect the relative fluxes seen in our sample which are plotted in Fig. B.1. We have attempted to quantify this for the different detectors used in the creation of our light curves. The sample of Sobolewska & Papadakis (2009) showed spectral changes with observed power-law slope varying between 1.0 and 2.0 (see their Fig. 7). For a typical Galactic absorption of 3×10^{20} cm^{-2} the change from slope of 1.0 to 2.0 would alter our estimated fluxes by −14% (ROSAT), −13% (*XMM-Newton*), +7% (*Swift*-XRT), +76% (*Suzaku*), +25% (Einstein-IPC). The change is large for *Suzaku* observations since in this case we use the count rate between 2.0–10.0 keV and extrapolate it to the soft band. All other satellites are sensitive in the soft band and hence the fluxes are less dependent upon the assumed spectral index. Six sources within our sample (XMMSL1 J024916.6-041244, J034555.1-355959, J045740.0-503053, J051935.5-323928, J070841.3-493305, and J193439.3+490922) display variation in flux of a factor of ten or greater between at least one pair of XMM and *Swift* observations, on timescales of months to years. The ratio between the soft X-ray flux observed with *Swift* and that observed with XMM for the remaining sources is typically a factor of a few. We observed the two TDE candidates with XRT, and found that both had faded significantly, following expectations from previous and later fluxes and upper limits (Figs. 1p and h).

[2] http://xmm.esac.esa.int/external/xmm_products/slew_survey/upper_limit/uls.shtml
[3] http://heasarc.gsfc.nasa.gov/Tools/w3pimms.html

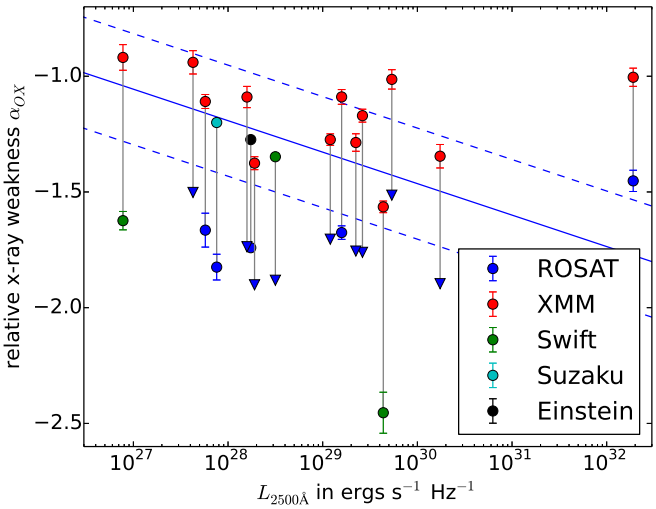

Fig. 4. Relative X-ray brightness α_{OX} plotted against luminosity $L_{2500\ \text{Å}}$ for the high-variability sample. For clarity only the brightest and faintest X-ray observations are shown. $L_{2500\ \text{Å}}$ is measured from the SED of each source and is assumed to be constant between observations. Triangles represent 95% upper limits.

6. Relative X-ray luminosity

Since the X-ray flux of AGN mainly consists of UV photons which gain energy in inverse Compton scattering processes the UV and the X-ray flux are closely correlated as described in Just et al. (2007). This allows us to estimate whether the X-ray luminosities of our sources are relatively bright or faint compared to AGN with the same UV luminosity. In Fig. 4 we compare the highest and lowest observed X-ray flux to the expected value using the relation given in Just et al. (2007), now omitting the two probable TDEs and the two probable spurious detections. The relative X-ray brightness α_{OX} is defined as

$$\alpha_{OX} = 0.3838 \cdot \log\left(\frac{F_{2\,\text{keV}}}{F_{2500\ \text{Å}}}\right), \quad (1)$$

where $F_{2\,\text{keV}}$ is the monochromatic flux at 2 keV and $F_{2500\ \text{Å}}$ the one at 2500 Å. Since the highest observed fluxes are usually XMM slew observations and the lowest ones either upper limits or observations with few counts, we can not use the spectra to determine the monochromatic flux at 2 keV. Instead we use PIMMS to obtain the flux F_{broad} between the energies $E_1 = 1.9$ keV and $E_2 = 2.1$ keV, assuming as before an absorbed power law with a photon index of $\Gamma = 1.7$. This result can be converted to the monochromatic flux at 2 keV using the relation

$$F_{2\,\text{keV}} = \frac{(2-\Gamma)E^{(1-\Gamma)}}{E_2^{(2-\Gamma)} - E_1^{(2-\Gamma)}} \cdot F_{\text{broad}}. \quad (2)$$

The flux at 2500 Å is approximated using measurements made by the XMM Optical Monitor, by the *Swift* UVOT or by Galex, depending on which is closest to the wavelength after considering the redshift of the AGN. For most sources, several measurements are available and we linearly interpolate the two data points which bracket the required wavelength, in double logarithmic space. If only one measurement exist we use this value. For two sources, XMMSL1 J044347.0+285822

Table 2. 2 keV: 2500 Å flux ratio α_{OX}.

XMMSL1 name	$\alpha_{OX,exp}$	$\alpha_{OX,min}$	$\alpha_{OX,max}$
J005953.1+314934	−1.2	−1.741 ± 0.008	−1.274 ± 0.005
J020303.1-074154	−1.2	≤−1.7	−1.09 ± 0.05
J024916.6-041244	−1.0	−1.62 ± 0.04	−0.92 ± 0.06
J034555.1-355959	–	–	–
J044347.0+285822	−1.2	−1.67 ± 0.07	−1.11 ± 0.03
J045740.0-503053	–	–	–
J051935.5-323928	−1.2	−1.82 ± 0.05	−1.20 ± 0.01
J064541.1-590851	–	–	–
J070841.3-493305	−1.4	−2.45 ± 0.09	−1.56 ± 0.03
J082753.7+521800	−1.4	≤−1.5	−1.01 ± 0.04
J090421.2+170927	−1.1	≤−1.5	−0.94 ± 0.05
J093922.5+370945	−1.4	≤−1.8	−1.17 ± 0.03
J100534.8+392856	−1.4	≤−1.8	−1.29 ± 0.04
J104745.6-375932	−1.3	≤−1.7	−1.27 ± 0.02
J112841.5+575017	−1.3	≤−1.9	−1.35 ± 0.01
J121335.0+325609	−1.4	−1.68 ± 0.03	−1.09 ± 0.03
J162553.4+562735	−1.5	≤−1.9	−1.35 ± 0.05
J173738.2-595625	−1.2	≤−1.9	−1.38 ± 0.03
J183521.4+611942	−1.8	−1.45 ± 0.05	−1.00 ± 0.04
J193439.3+490922	–	–	–

Notes. Columns give the source name, the expected α_{OX} for a source with this $L_{2500\ Å}$ from the correlation of Steffen et al. (2006), α_{OX} calculated from the minimum X-ray flux and α_{OX} calculated from the maximum X-ray flux that we have recorded for that particular source.

and XMMSL1 J173738.2-595625, there are no reasonably close measurements available and we estimate a value by extrapolating the SED by eye. For those two cases the numbers have to be treated as an order of magnitude estimate, while for the other AGN we estimate the uncertainties on the UV flux, introduced by the interpolation, to be ≤0.1 dex. Since the UV light is heavily affected by extinction, we need to correct for the Galactic hydrogen column density (Schlegel et al. 1998). It would be preferable to consider intrinsic absorption as well, however as mentioned above for most of those data points no spectra are available, such that we have no information about intrinsic absorbers. The X-ray fluxes are also corrected for Galactic absorption. We note that the UV and X-ray data are typically not simultaneous, and as these are variable sources this could, in principle, introduce errors on our measured values of α_{OX}. In practice, X-ray variability tends to be much greater than UV variability (e.g. Grupe et al. 2012; Saxton et al. 2014) and so changes in α_{OX} will be dominated by the X-ray luminosity. Our calculated values are given in Table 2. We are now able to say how the different X-ray observations of our sources compare to other AGN which have the same UV luminosity. In Fig. 4 we show the relative X-ray luminosity for the brightest and the faintest X-ray observations and the values for the individual sources are also given in Table 2. The straight line is the relation between α_{OX} and UV luminosity, found for an optically-selected sample of 333 AGN by Steffen et al. (2006), with the 1σ deviations indicated. Radio-loud sources are relatively X-ray bright (Gibson et al. 2008), since additional X-rays arise from the jet activity, and are expected to deviate from this relation. Indeed the two radio loud sources of our sample lie clearly above the relation. These are XMMSL1 J082753.7+521800 with a UV luminosity of $10^{29.6}$ erg s^{-1}Hz^{-1} and XMMSL1 J183521.4+611942, the blazar at the highest UV luminosity. For the other sources we summarise that in nearly all cases their most luminous observation corresponds to the expected X-ray luminosity, while in their faintest states they are X-ray weak. We note that none of our non-radio-loud sources have been observed to be X-ray bright. One source, 1H 0707-495, with $\log L_{2500\ Å} = 29.5$ erg, reaches very low values of α_{OX}. This low state has been attributed to a collapse of the X-ray corona to a region so close to the black hole that only a few hard X-rays escape (Fabian et al. 2012). Dong et al. (2012) analysed a sample of 49 optically selected, low-mass, narrow-line AGN with UV luminosities in the range 10^{27-28} erg s^{-1}Hz^{-1}. They found that nearly 50% of their sources lie below the 1σ-region of the relation from Steffen et al. (2006). Their result may well be explained by X-ray variability.

7. Spectral analysis

The high-variability sample has been selected from ROSAT-XMM variability. To attempt to understand the variability mechanism in each source, it is essential to have spectral information at high and low fluxes, covering an energy band broad enough to constrain absorbing column densities. This is possible for the pointed XMM and *Swift* spectra of our sources but not for the earlier ROSAT low-energy spectra or upper limits and for most of the slew observations. While all of our sources have undergone extreme variability in the past, all except six sources show less extreme variations between the slew and *Swift* observations, common among AGN on months-year timescales. We analyse the X-ray spectra of *Swift* observations from our programme using the full spectral range from 0.3–10.0 keV and using models available in Xspec. Many of the spectra suffer from low statistics, such that complex models are poorly constrained. A simple power law model with Galactic absorption is a reasonable fit for most of the spectra (using Cash statistics, see Table B.1). Below we explore whether a cold or an ionised absorber can explain the observed variability. Some of our sources have been observed by XMM in pointed observations. We consider the additional spectra as well as published results in comparison with the observations of this programme. By applying the more complex models of the high quality spectra to our observations, we can observe how the parameters of the model change. The results of the spectral fits for individual sources are discussed in Appendix A. The parameters of the best fitting models are given in Table B.1. The spectra of XMMSL1 J024916.6-041244 are of particular interest being very soft and lacking the usual power-law emission seen above 2 keV. This source is discussed further in Appendix A.4.

7.1. Neutral absorber

One obvious reason for variability is a change in absorption along the line-of-sight. In order to quantify whether this is a possible explanation for the change in brightness of our sources, we check whether the spectra are compatible with thick enough absorbers to explain the observed variability. We add a further, intrinsic neutral absorber to account for absorption in excess of that of our Galaxy using the xspec model *zpcfabs* for a partially covering neutral absorber at the source distance. We fix the absorber's covering fraction to one in order to reduce the number of free model parameters to explain a large flux change. Such a partially covering absorber has a similar spectral signature to a completely covering absorber and so would be found with this method. The effect of a neutral or ionised absorber on the spectrum can be seen in Fig. 5. The redshift is set to the source redshift or to $z = 0.05$ if the redshift is unkown. The spectra of all sources except XMMSL1 J044347.0+285822 are fit best without any additional neutral absorption. We apply the largest column density allowed at the 90% level and compare the soft flux of the absorbed spectrum to the soft flux

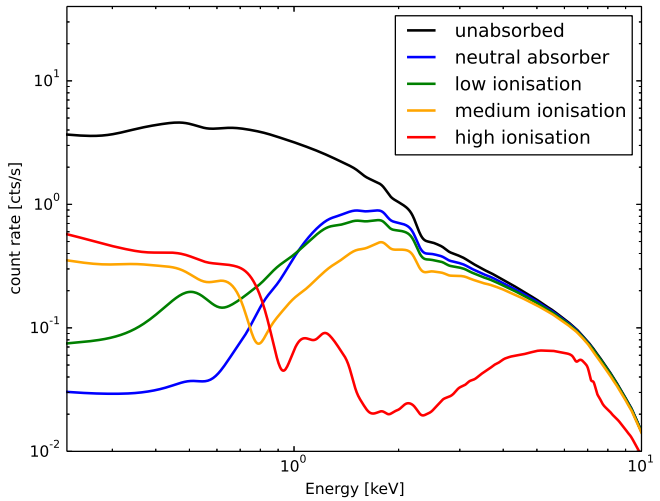

Fig. 5. Effect of absorption on a power law spectrum of $\Gamma = 1.7$ and Galactic absorption of $N_{\rm H} = 3 \times 10^{20}$cm^{-2} here adopting the effective area of XMM. Absorbers with various ionisation parameters have been tuned such that the soft (0.2–2 keV) X-ray flux is reduced by a factor ten. The necessary column densities are 0.89×10^{22} cm^{-2} for the neutral absorber, 0.67×10^{22} cm^{-2} for low ionisation ($\log(\xi) = -1$), 2.26×10^{22} cm^{-2} for medium ionisation ($\log(\xi) = 0.5$) and 36.1×10^{22} cm^{-2} for high ionisation ($\log(\xi) = 2$).

without the additional absorber. Assuming that the brightest observed flux corresponds to the unobscured source, we check whether the obtained column densities are high enough to account for the difference between the brightest point and the flux measured in the *Swift* follow-up observation. In general the photon index is a free parameter in this fit but for several poorly constrained spectra we fix it to 1.7 to avoid unphysical results. The results of the calculations are shown in Table B.2. In most cases, absorption by neutral hydrogen does not offer an explanation for the observed variability. Only one source, XMMSL1 J044347.0+285822, is consistent with a high column density of neutral hydrogen, that can account for the observed flux change. Indeed for this source, the detailed analysis of the XMM pointed observation spectrum indicates that there are several neutral partially covering absorbers (Ricci et al. 2010) in the line-of-sight. In two cases, XMMSL1 J064541.1-590851 and XMMSL1 J112841.5+575017, the *Swift* observation is of similar strength to the brightest observed point such that small column densities are sufficient to explain the rather small variability between those two points. For those cases absorption can not be excluded, as the *Swift* spectrum might correspond to a nearly unobscured state. Two sources, 1H 0707-495 and XMMSL1 J024916.6-041244, have spectra that deviate significantly from an absorbed power law. Here we do not consider those two sources since we can not obtain a good fit with an absorbed power law model. The source 1H 0707-495's variability is likely due to its changing corona (see Sect. A.10 for a summary). The emission of XMMSL1 J024916.6-041244 seems to be purely thermal (see Sect. A.4). Please note that the observed flux ratios in Table B.2 correspond to the numbers shown in Fig. B.1. We hence assumed that the spectral shape between the observations does not change, which of course is not true for variable absorption. Variable absorbers can change the effective spectral index in the soft band. The resulting errors on the flux rates are quantified in Sect. 5.

7.2. Ionised absorber

An alternative to intrinsic neutral absorption is to consider absorption by warm, ionised gas, which leads to a different spectral signature as shown in Fig. 5. To test this possibility, we use the Xspec *zxipcf* model where, as before, we fix the covering fraction and redshift. The absorption also depends on the degree of ionisation $\log(\xi)$ as can be seen in Fig. 5. Many of our spectra are, however, not good enough to fit the ionisation fraction reliably. We therefore chose three different ionisation levels which we use in the fits. Highly ionised gas absorbs less efficiently at soft energies; for $\log(\xi) = 3$ even a huge column density of $N_{\rm H} = 5 \times 10^{24}$ cm^{-2} only reduces the 0.2–2 keV flux by a factor of four. Since in general we see higher variations, these are unlikely to be caused by such highly ionised gas clouds. We therefore only use lower ionisations of $\log(\xi) = 2$, $\log(\xi) = 0.5$ and $\log(\xi) = -1$. For even lower values the effect of the absorber would be similar to that of a neutral absorber. In Table B.3, we quote the results for the ionisation degree that leads to the highest absorption. Five of the spectra require an ionised absorber when fitted with a power law model. These are: XMMSL1 J020303.1-074154, XMMSL1 J024916.6-041244, XMMSL1 J044347+285822, where a neutral absorber is preferred (see Appendix A.6), XMMSL1 J090421.2+170927, and XMMSL1 J121335.0+325609. The analysed *Swift* spectrum of XMMSL1 J020303.1-074154 is best described with a highly ionised absorber though this cannot account for the observed flux change (see Appendix A.3). When using a power law model, the fit to the *Swift* spectrum of XMMSL1 J024916.6-041244 is improved by adding an ionised absorber. The pointed XMM observation of the source is, however, best described by a pure black body model which implies thermal emission instead (compare Appendix A.4). The absorber required by the spectrum of XMMSL1 J090421.2+170927 can explain variability by a large factor (of up to seven) and there are no further spectra which could indicate a different explanation. For this source absorption by ionised material might hence explain the observed variability. For XMMSL1 J121335.0+325609 the situation is comparable to XMMSL1 J020303.1-074154: Some ionised absorption improves the fit, however the spectrum is not consistent with a large enough column density to explain the observed variability. In addition there are four sources (XMMSL1 J064541.1-590851, XMMSL1 J082753.7+521800, XMMSL1 J100534.8+392856, and J104745.6-375932) where an additional ionised absorber does not improve the fit, however the absorption allowed at the 90% level is sufficient to explain the relatively small differences between the analysed spectra and the brightest observations. Hence, we found one source, XMMSL1 J090421.2+170927, where absorption by ionised gas is a likely explanation for the observed variability. Two further sources might exhibit ionised absorbers, though these are not massive enough to be the only reason for the variability. Moreover there are four sources where we can not rule out variable ionised absorption as the reason for small flux changes between the analysed spectra and the brightest observation. In summary there is little direct evidence that variability is caused by absorption effects, a conclusion also reached by Sobolewska & Papadakis (2009) in an analysis of RXTE AGN observations.

8. Discussion

We have defined a complete sample of candidate highly variable AGN within the *XMM-Newton* slew survey, and followed

these up with the *Swift* satellite. Together with archival data, we have used the temporal and spectral information to identify potential variability mechanisms, and to better understand the variable AGN population.

8.1. Highly variable AGN as a population

The XMM slew survey AGN sample (Saxton et al. 2011) is dominated (~80%) by sources which are constant within a factor of three, and just 5% can be classed as highly variable (flux changes of a factor of ten or more). Among the highly variable sample we present here, a small number are drawn from rare types: we find one (possibly two) blazars (XMMSL1 J183521.4+611942 and maybe XMMSL1 J082753.7+521800), one low-mass, extremely soft source (XMMSL1 J024916.6-041244) and two nearby tidal disruption candidates (XMMSL1 J111527.3+180638 and XMMSL1 J132342.3+482701). An overview of the possible variability mechanisms is presented in Table A.2. Disregarding the two spurious detections, the remainder appear to be more typical AGN, spanning a wide range of types including QSO, Seyfert 1, Seyfert 1.5, Seyfert 2 and NLS1. Therefore, the sources in this highly variable sample do not appear to be a fundamentally different class, but are drawn from all AGN populations. The spread in black hole masses for the sample supports this idea (Table 1). They are, however, marginally more likely to be found at lower redshifts. We do not find any unusually X-ray bright AGN among the highly variable sample, and at their faintest, these sources are generally X-ray weak. We confirm that in their brightest states the X-ray fluxes are consistent with other AGN with the same UV luminosity. Many of the AGN go through more than one high and low state between the ROSAT and latest *Swift* observations, but a small number (XMMSL1 J064541.1-590851, J100534.8+392856 and J112841.5+575017) initially observed at faint fluxes, brightened, and remained at the same flux level in subsequent observations. These are what Kanner et al. (2013) call state-change objects, which should not be confused with the state-changes reported in Galactic black-hole binary systems that are due to disc structure changes (Esin et al. 1997). Although our detection method is well suited for finding AGN which have transited into the high-soft state, we do not find any such AGN, which suggests that such transitions are either very rare or very slow (but see Miniutti et al. 2013).

8.2. Variable absorption

To investigate the cause of the variability we examined absorption in the available spectra. Among the 18 sources with spectra, only XMMSL1 J044347.0+285822 can be variable due to neutral obscuration alone, while XMMSL1 J090421.2+170927 might feature a moderately ionised absorber thick enough to explain the variation of a factor of approximately six compared to its brightest point. More complicated absorption models could possibly explain the variability of the Sy 1.2, XMMSL1 J005931.1+314934 (see Appendix A.1) and of the Sy 1.5, XMMSL1 J051935.5-323928 (Agís-González et al. 2014). Our conclusion is thus that for a subsample of our sources (one quarter) the variability is likely to be as a result of changing absorbers. The other sources are likely to exhibit absorption to some degree (see Tables B.2 and B.3), although the column densities are not high enough to explain the factors of ten or more variability observed at earlier epochs (between ROSAT and XMM), implying that for most sources an additional mechanism is required.

8.3. Variable intrinsic emission

If the observed behaviour is not due to absorption, it must be due to variable emission. We have approximated the AGN spectra with a simple power law model when comparing fluxes but actual spectra are more complex, typically showing excess emission above an extension of the power law below 1–2 keV (e.g. Comastri et al. 1992; Saxton et al. 1993; Scott et al. 2012). The nature of this soft excess is not agreed upon in the literature and may vary from source to source. Candidate mechanisms include thermal emission from the inner region of the accretion disc, relevant for low-mass BH (Yuan et al. 2010; Terashima et al. 2012; Miniutti et al. 2013), a low-electron-temperature Comptonisation zone (Done et al. 2012) or relativistically blurred reflection of the primary power law continuum from the inner disc (George & Fabian 1991; Fabian et al. 1989) where the strong variability may be enhanced by gravitational amplification (Miniutti & Fabian 2004). Based on the X-ray spectra, XMMSL1 J024916.6-041244 is a strong candidate for variability caused by changes in thermal disc emission. This ties in with it being the lowest-mass BH in our sample; none of the other sources show evidence for thermal emission. Variable disc reflection is a more widely-applicable mechanism, previously cited for the spectral and temporal variations of XMMSL1 J070841.3-493305 (Fabian et al. 2009, 2012) and proposed for strong variability seen in PHL 1094 (Miniutti et al. 2009, 2012), Mrk 335 (Gallo et al. 2013), and PG 2112+059 (Schartel et al. 2010) among others. Here, the flux and spectral variability is attributed to the expansion and contraction of a comptonising electron cloud, leading to a highly variable disc reflection (Wilkins & Gallo 2015). It is difficult to discriminate between complex absorption and blurred reflection models purely from the medium-energy X-ray spectrum. Studies with *NuSTAR* have broken the degeneracy by providing compelling evidence for a Compton hump at higher energies, consistent with the reflection model (Parker et al. 2014; Wilkins et al. 2015).

8.4. Spurious sources and unconfirmed AGN

We conclude that two of our candidate AGN are in fact spurious detections in the slew survey because no other X-ray detection was made and no nearby multiwavelength catalogued counterparts could be found. The detection likelihood of XMMSL1 J015510.9-140028 was the lowest of our sample and close to the lower limit required for the Clean catalogue[4]. While on visual inspection, XMMSL1 J113001.8+020007 does not appear to have the profile of a typical point source. Furthermore, they both have quite a large offset from their nearest SDSS galaxy counterpart (0.3 and 0.2 arcmin). It is possible that these sources are normally very faint, and are bona fide transients, but the lack of subsequent detections together with the large offset to the counterpart makes it likely that these are indeed spurious. Four of our sources, excluding the spurious detections, are associated with galaxies with no known redshift. All of these have counterparts in 2MASS and WISE with IR colours that indicate an AGN nature and rule out a stellar classification, using the technique illustrated in the slew hard band survey (see Fig. 7 of Warwick et al. 2012, for a comparison) and a sample of unidentified transients in the slew survey (Starling et al. 2011). We show the results in Fig. 6. In two cases, XMMSL1 J064541-590851 and XMMSL1 J121335.0+325609,

[4] The *Clean* slew survey catalogue contains sources with detection likelihoods >10 (see Saxton et al. 2008).

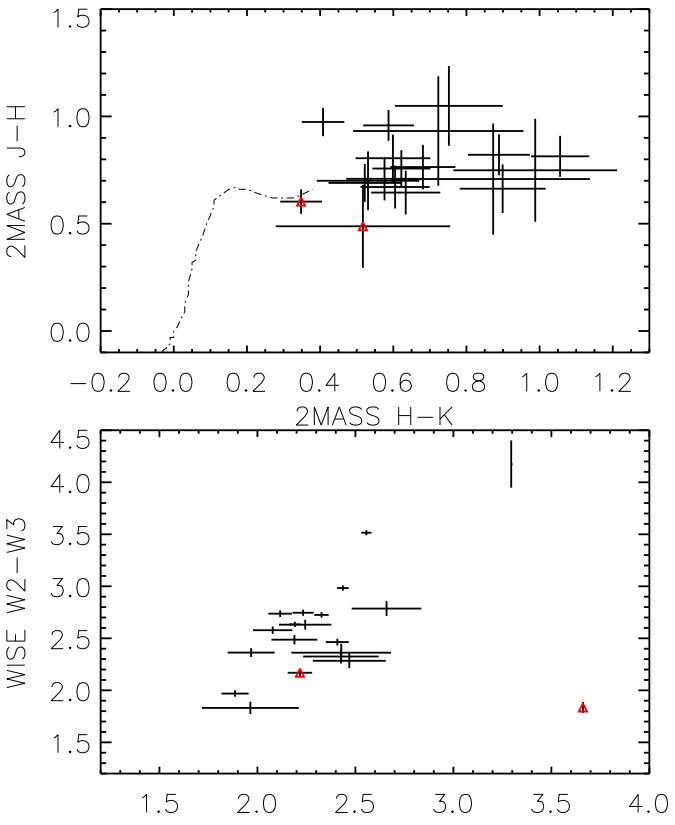

Fig. 6. 2MASS (*upper panel*) and WISE (*lower panel*) colours of all sources in our sample detected in both infrared surveys. Candidate TDEs are marked with red triangles. The black dashed line in the upper plot indicates the expected colours for main sequence stars, while colours to the upper right of the end of this line are typical of AGN. All the WISE colours we find are consistent with an AGN or galaxy nature, and stellar colours would lie off the plot to the bottom left.

there are two possible counterparts, within the XMM slew error circle. For XMMSL1 J121335.0+325609 both of these are consistent with an AGN source, while the 2MASS colours for XMMSL1 J064541-590851 indicate that one of the possible counterparts (the fainter one) has colours typical of a star on the main sequence. We have used the more accurate position of the *Swift*-XRT observation to narrow the match down to just one candidate, an AGN, in both of these sources.

8.5. Conclusions

We have investigated the properties of a well-determined sample of AGN selected on the basis of their long-term X-ray variability. After removal of two spurious detections the sample spans a wide range of optical classifications and appears to be drawn from the general AGN population, albeit with a slightly lower average redshift and luminosity than a non-varying control sample. Of the 22 AGN, two are radio-loud and most probably vary due to jet activity, two are candidate tidal disruption events, four show variable neutral or multi-phase absorption, the lowest mass object has variable intrinsic thermal disc emission and the well-studied variability in the NLS1 XMMSL1 J070841.3-493305 has been attributed elsewhere to reflection from a changing comptonising, power law emission component. We cannot say with confidence what the variability mechanism is for the remaining sources. We see that the peak X-ray flux is consistent with that expected from the UV luminosity but in the lowest flux measurements the sources are generally X-ray weak. This may indicate absorption although we can exclude changes in a single component absorber in most cases. Changes in multiple absorbers cannot be excluded with our data and provide perhaps the most likely explanation for the two Seyfert 2 galaxies (XMMSL1 J112841.5+575017 and J173739.3-595625). The NLS1 XMMSL1 J093922.5+370945 might share the same variability mechanism as J070841.3-493305. A summary of proposed variability mechanisms is given in Table A.2. A larger sample, extracted from future releases of the XMM slew survey or from dedicated survey instruments, such as *eRosita* (Predehl et al. 2010), will be useful to further investigate differences in the variable AGN population.

Acknowledgements. N.L.S. was supported by the ESAC traineeship programme. R.L.C.S. was supported by a Royal Society Dorothy Hodgkin Fellowship. PAE acknowledges support from the UK Space Agency. We thank Kim Page for assistance with the *Swift* data. This work made use of data supplied by the UK *Swift* Science Data Centre at the University of Leicester. The *XMM-Newton* project is an ESA science mission with instruments and contributions directly funded by ESA member states and the USA (NASA). This research has made use of the NASA/IPAC Extragalactic Database (NED) which is operated by the Jet Propulsion Laboratory, California Institute of Technology, under contract with the National Aeronautics and Space Administration. This publication makes use of data products from the Wide-field Infrared Survey Explorer, which is a joint project of the University of California, Los Angeles, and the Jet Propulsion Laboratory/California Institute of Technology, funded by the National Aeronautics and Space Administration. This publication makes use of data products from the Two Micron All Sky Survey, which is a joint project of the University of Massachusetts and the Infrared Processing and Analysis Center/California Institute of Technology, funded by the National Aeronautics and Space Administration and the National Science Foundation.

References

Agís-González, B., Miniutti, G., Kara, E., et al. 2014, MNRAS, 443, 2862
Arcavi, I., Gal-Yam, A., Sullivan, M., et al. 2014, ApJ, 793, 38
Barthelmy, S. D., Barbier, L. M., Cummings, J. R., et al. 2005, Space Sci. Rev., 120, 143
Baumgartner, W. H., Tueller, J., Markwardt, C. B., et al. 2013, ApJS, 207, 19
Boller, T., Brandt, W. N., Fabian, A. C., & Fink, H. H. 1997, MNRAS, 289, 393
Burrows, D. N., Hill, J. E., Nousek, J. A., et al. 2005, Space Sci. Rev., 120, 165
Caramete, L. I., & Biermann, P. L. 2010, A&A, 521, A55
Comastri, A., Setti, G., Zamorani, G., et al. 1992, ApJ, 384, 62
Dauser, T., Svoboda, J., Schartel, N., et al. 2012, MNRAS, 422, 1914
Done, C., Davis, S. W., Jin, C., Blaes, O., & Ward, M. 2012, MNRAS, 420, 1848
Dong, R., Greene, J. E., & Ho, L. C. 2012, ApJ, 761, 73
Esin, A. A., McClintock, J. E., & Narayan, R. 1997, ApJ, 489, 865
Esquej, P., Saxton, R. D., Freyberg, M. J., et al. 2007, A&A, 462, L49
Esquej, P., Saxton, R. D., Komossa, S., et al. 2008, A&A, 489, 543
Evans, P. A., Beardmore, A. P., Page, K. L., et al. 2009, MNRAS, 397, 1177
Evans, P. A., Osborne, J. P., Beardmore, A. P., et al. 2014, ApJS, 210, 8
Fabian, A. C., Rees, M. J., Stella, L., & White, N. E. 1989, MNRAS, 238, 729
Fabian, A. C., Zoghbi, A., Ross, R. R., et al. 2009, Nature, 459, 540
Fabian, A. C., Zoghbi, A., Wilkins, D., et al. 2012, MNRAS, 419, 116
Gallo, L. C., Fabian, A. C., Grupe, D., et al. 2013, MNRAS, 428, 1191
Gehrels, N., Chincarini, G., Giommi, P., et al. 2004, ApJ, 611, 1005
George, I. M., & Fabian, A. C. 1991, MNRAS, 249, 352
Gezari, S., Basa, S., Martin, D. C., et al. 2008, ApJ, 676, 944
Gibson, R. R., Brandt, W. N., & Schneider, D. P. 2008, ApJ, 685, 773
Greene, J. E., & Ho, L. C. 2007, ApJ, 667, 131
Greiner, J., Schwarz, R., Zharikov, S., & Orio, M. 2000, A&A, 362, L25
Grupe, D., Beuerman, K., Mannheim, K., et al. 1995, A&A, 300, L21
Grupe, D., Komossa, S., Gallo, L. C., et al. 2012, ApJS, 199, 28
Ho, L. C., Darling, J., & Greene, J. E. 2008, ApJS, 177, 103
Ho, L. C., Kim, M., & Terashima, Y. 2012, ApJ, 759, L16
Just, D. W., Brandt, W. N., Shemmer, O., et al. 2007, ApJ, 665, 1004
Kanner, J., Baker, J., Blackburn, L., et al. 2013, ApJ, 774, 63
Komossa, S. 2015, J. High Energy Astrophysics, 7, 148
Komossa, S., & Bade, N. 1999, A&A, 343, 775
Komossa, S., & Fink, H. 1997, in IAU Colloq. 159: Emission Lines in Active Galaxies: New Methods and Techniques, eds. B. M. Peterson, F.-Z. Cheng, & A. S. Wilson, ASP Conf. Ser., 113, 246

Komossa, S., Zhou, H., Wang, T., et al. 2008, ApJ, 678, L13
Lin, D., Irwin, J. A., Godet, O., Webb, N. A., & Barret, D. 2013, ApJ, 776, L10
MacLeod, C. L., Ivezić, Ž., Kochanek, C. S., et al. 2010, ApJ, 721, 1014
Maksym, W. P., Ulmer, M. P., & Eracleous, M. 2010, ApJ, 722, 1035
Marconi, A., & Hunt, L. K. 2003, ApJ, 589, L21
Markowitz, A. G., Krumpe, M., & Nikutta, R. 2014, MNRAS, 439, 1403
McHardy, I. M., Uttley, P., Taylor, R. D., & Seymour, N. 2004, in X-ray Timing 2003: Rossi and Beyond, eds. P. Kaaret, F. K. Lamb, & J. H. Swank, AIP Conf. Ser., 714, 174
McHardy, I. M., Koerding, E., Knigge, C., Uttley, P., & Fender, R. P. 2006, Nature, 444, 730
Miniutti, G., & Fabian, A. C. 2004, MNRAS, 349, 1435
Miniutti, G., Fabian, A. C., Brandt, W. N., Gallo, L. C., & Boller, T. 2009, MNRAS, 396, L85
Miniutti, G., Brandt, W. N., Schneider, D. P., et al. 2012, in EPJ Web Conf., 39, 6002
Miniutti, G., Saxton, R. D., Rodríguez-Pascual, P. M., et al. 2013, MNRAS, 433, 1764
Nandra, K. 2001, Adv. Space Res., 28, 295
O'Neill, P. M., Nandra, K., Papadakis, I. E., & Turner, T. J. 2005, MNRAS, 358, 1405
Panessa, F., Bassani, L., Cappi, M., et al. 2006, A&A, 455, 173
Parisi, P., Masetti, N., Jiménez-Bailón, E., et al. 2009, A&A, 507, 1345
Parker, M. L., Wilkins, D. R., Fabian, A. C., et al. 2014, MNRAS, 443, 1723
Parker, M. L., Fabian, A. C., Matt, G., et al. 2015, MNRAS, 447, 72
Ponti, G., Papadakis, I., Bianchi, S., et al. 2012, A&A, 542, A83
Predehl, P., Andritschke, R., Böhringer, H., et al. 2010, in Space Telescopes and Instrumentation 2010: Ultraviolet to Gamma Ray, SPIE Conf. Ser., 7732, 77320
Rees, M. J. 1988, Nature, 333, 523
Ricci, C., Beckmann, V., Audard, M., & Courvoisier, T. J.-L. 2010, A&A, 518, A47
Risaliti, G., Elvis, M., & Nicastro, F. 2002, ApJ, 571, 234
Risaliti, G., Elvis, M., Fabbiano, G., Baldi, A., & Zezas, A. 2005, ApJ, 623, L93
Roming, P. W. A., Kennedy, T. E., Mason, K. O., et al. 2005, Space Sci. Rev., 120, 95
Saxton, R. D., Turner, M. J. L., Williams, O. R., et al. 1993, MNRAS, 262, 63
Saxton, R. D., Read, A. M., Esquej, P., et al. 2008, A&A, 480, 611
Saxton, R., Read, A., Esquej, P., Miniutti, G., & Alvarez, E. 2011, ArXiv e-prints [arXiv:1106.3507]
Saxton, R. D., Read, A. M., Esquej, P., et al. 2012, A&A, 541, A106
Saxton, R. D., Read, A. M., Komossa, S., et al. 2014, A&A, 572, A1
Schartel, N., Rodríguez-Pascual, P. M., Santos-Lleó, M., et al. 2010, A&A, 512, A75
Schlegel, D. J., Finkbeiner, D. P., & Davis, M. 1998, ApJ, 500, 525
Scott, A. E., Stewart, G. C., & Mateos, S. 2012, MNRAS, 423, 2633
Shappee, B. J., Prieto, J. L., Grupe, D., et al. 2014, ApJ, 788, 48
Shen, Y., Greene, J. E., Strauss, M. A., Richards, G. T., & Schneider, D. P. 2008, ApJ, 680, 169
Simien, F., & de Vaucouleurs, G. 1986, ApJ, 302, 564
Sobolewska, M. A., & Papadakis, I. E. 2009, MNRAS, 399, 1597
Soldi, S., Beckmann, V., Baumgartner, W. H., et al. 2014, A&A, 563, A57
Starling, R. L. C., Evans, P. A., Read, A. M., et al. 2011, MNRAS, 412, 1853
Starling, R. L. C., Done, C., Jin, C., et al. 2014, MNRAS, 437, 3929
Steffen, A. T., Strateva, I., Brandt, W. N., et al. 2006, AJ, 131, 2826
Tatum, M. M., Turner, T. J., Miller, L., & Reeves, J. N. 2013, ApJ, 762, 80
Terashima, Y., Kamizasa, N., Awaki, H., Kubota, A., & Ueda, Y. 2012, ApJ, 752, 154
Terrano, W. A., Zaw, I., & Farrar, G. R. 2012, ApJ, 754, 142
Turner, T. J., & Pounds, K. A. 1989, MNRAS, 240, 833
van Velzen, S., Farrar, G. R., Gezari, S., et al. 2011, ApJ, 741, 73
Véron-Cetty, M.-P., & Véron, P. 2006, A&A, 455, 773
Voges, W., Aschenbach, B., Boller, T., et al. 1999, VizieR Online Data Catalog: IX/10
Warwick, R. S., Saxton, R. D., & Read, A. M. 2012, A&A, 548, A99
Wilkins, D. R., & Gallo, L. C. 2015, MNRAS, 449, 129
Wilkins, D. R., Gallo, L. C., Grupe, D., et al. 2015, MNRAS, 454, 4440
Willingale, R., Starling, R. L. C., Beardmore, A. P., Tanvir, N. R., & O'Brien, P. T. 2013, MNRAS, 431, 394
Winter, L. M. 2010, ApJ, 725, L126
Winter, L. M., Mushotzky, R. F., Reynolds, C. S., & Tueller, J. 2009, ApJ, 690, 1322
Winter, L. M., Veilleux, S., McKernan, B., & Kallman, T. R. 2012, ApJ, 745, 107
Yuan, W., Liu, B. F., Zhou, H., & Wang, T. G. 2010, ApJ, 723, 508
Zhou, X.-L., & Soria, R. 2013, in IAU Symp. 290, eds. C. M. Zhang, T. Belloni, M. Méndez, & S. N. Zhang, 371

Appendix A: Individual sources

We now summarise the results for each source individually, providing further detailed information in some cases, and list the conclusions in Table A.2.

A.1. XMMSL1 J005953.1+314934

This Seyfert 1.2 galaxy is well known and several spectra are available. Over the last 30 years it has experienced several bright and dim states. No publication dedicated to this source is available but it has been used in a sample to support the model of multi-cloud absorption (Tatum et al. 2013). Apart from the slew spectrum, three rather good quality spectra are available. We fit the best one, the pointed XMM observation from January 2006, and compared the residuals of the other spectra relative to this fit. The XMM spectrum can be reasonably well fit by a simple model of a power law plus a black body (kT = 120 eV) and Galactic absorption. The XMM spectrum corresponds to a rather bright state, a factor of seven brighter than the dimmest observation. In Fig. A.1, the *Swift* spectrum from June 2006 looks to be absorbed, while the later *Swift* spectrum and earlier XMM slew survey spectrum do not deviate much from the XMM pointed observation. We did not reanalyse the *Suzaku* spectrum from 2010 here but according to Winter et al. (2012) it can also be fitted with a power law and a soft black body, so it is probably similar to the XMM spectrum. This is consistent with the light curve (Fig. B.1a), where the June 2006 observation exhibits a flux lower by a factor of three compared to the XMM observation from five months earlier, while in all other spectra the AGN had roughly the same luminosity.

Motivated by this observation, we tried to find an absorption model that can be applied to all spectra. A better fit to the 2006 XMM spectrum is achieved by adding a partially covering neutral as well as an ionised absorber with the parameters given in Table B.1. Since the other spectra have fewer counts we freeze as many parameters as possible. The *Swift* 2006 observation can be fitted with the model from the XMM 2006 spectrum by adjusting only the covering fractions of the two absorbers and the normalisation of the power law. The covering fraction of the neutral absorber rises from 36% to 50%, which explains the dimming, while the ionised absorber is no longer needed. The two other spectra are less constrained. They can both be fitted by changing the covering fraction of the neutral absorber, but they cannot constrain the ionised one. All fit parameters are given in Table B.1. We conclude that this AGN's variability is probably due to absorption by both neutral and ionised partially covering absorbers. There are UVOT observations in the u band for both *Swift* observations. For the 2006 observation which is absorbed in X-rays the UV flux is lower by 30%. This is most probably due to the presence of the absorber, which covers the UV emitting region partially. It has been variously shown in the literature that multi-phase absorption cannot be spectrally distinguished from emission because of relativistically-blurred disc reflection in the 0.2–10 keV band. In the case of XMMSL1 J00534.8+392856 the significant change in UV flux may make it more likely that the variability seen here is due to absorption rather than reflection.

A.2. XMMSL1 J015510.9-140028

This source was only detected in the XMM slew survey being just above the detection threshold. Since it could not be found before or after that and does not have a counterpart in other wavelength bands, other than a rather distant (offset = 20″) galaxy, APMUKS(BJ) B015244.14-141523.0, we assume that it is a false detection.

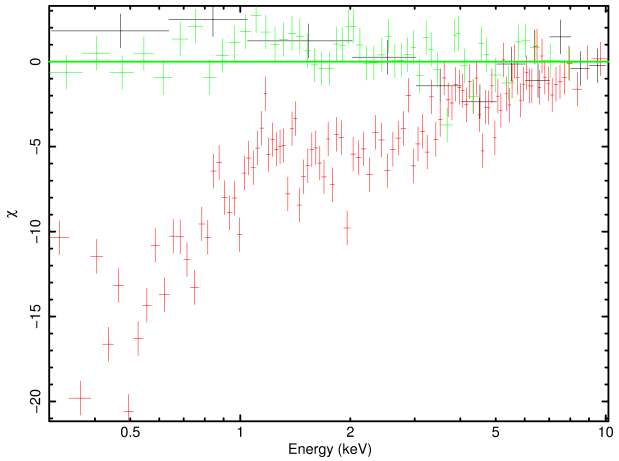

Fig. A.1. Residuals of the XMM slew 2002 (black), *Swift* 2006 (red) and *Swift* 2011 (green) observations of XMMSL1 J00534.8+392856 when compared to the best fit to the XMM spectrum of 2006, a simple power law plus a black body model.

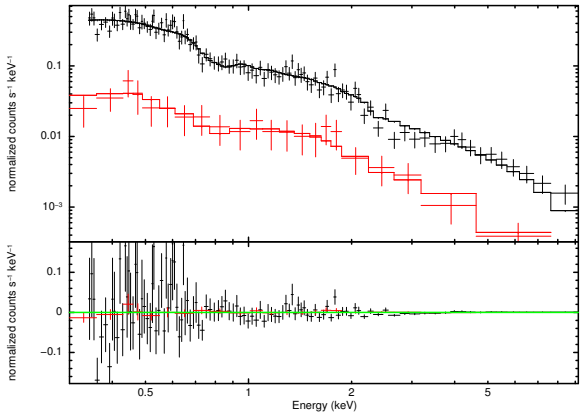

Fig. A.2. Simultaneous fit of the XMM 2006 and the merged *Swift* spectra of XMMSL1 J020303.1-074154. The model consists of a power law with $\Gamma = 2.29^{+0.07}_{-0.05}$ and a strongly ionised thick absorber with $\log(\xi) = 1.97^{+0.14}_{-0.19}$ and $N_{\rm H} = 2.8^{+1.0}_{-0.5} \times 10^{22}$ cm^{-2}. All parameters are the same for both models, except the normalisation, which is 40% larger for the merged *Swift* spectra.

A.3. XMMSL1 J020303.1-074154

After brightening in 2004 the source was found to remain in a rather constant luminosity state a factor of five below the XMM slew observation. The spectrum of the XMM pointed observations is best fit with an ionised absorber. However some residuals remain in the spectrum and removing the absorber only increases the soft flux by 40%. The *Swift* spectra are all quite similar and we merge these to improve statistics before comparing with the XMM spectrum, which can be fitted with the same model but with lower normalisation, in Fig. A.2. The soft absorber we found is not thick enough to explain the high variability and the mechanism remains unclear.

A.4. XMMSL1 J024916.6-041244

The long-term light curve consists of a single flare which faded over a number of years. The underlying spectrum is soft and

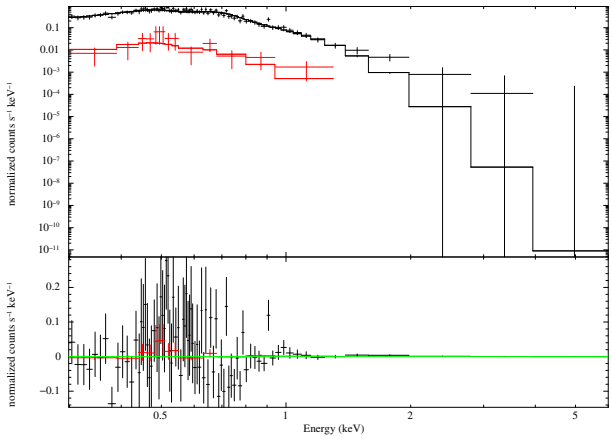

Fig. A.3. Simultaneous fit of an absorbed black body model to XMM pointed (black) and *Swift*-XRT (red) observations of XMMSL1 J024916.6-041244. The black body temperature and normalisation is independent in each fit while the absorption has been tied.

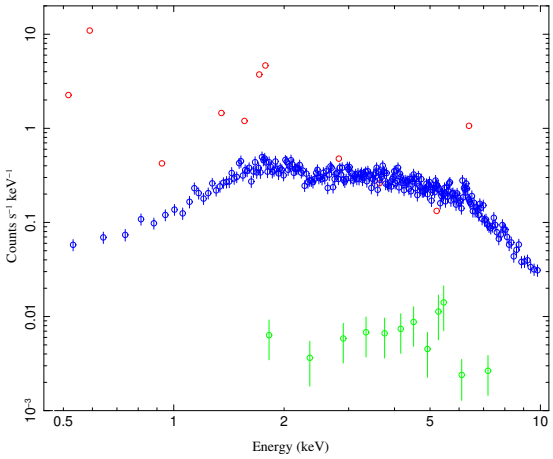

Fig. A.4. Spectra of XMMSL1 J044347.0+285822 from the slew survey 2003 (red), from an XMM pointed observation 2007 (blue) and during the *Swift* follow-up observation in 2010 (green). Please note that the spectra are not relatively calibrated.

seems to be predominantly thermal. An XMM pointed observation may be fit by a black body, of temperature kT = 110−140 eV, absorbed by both cold ($N_{\rm H}$ ∼ 10^{21} cm^{-2}) and ionised ($N_{\rm H}$ ∼ 6×10^{23} cm^{-2}; log(ξ) ∼3) gas. A later *Swift*-XRT spectrum, shows a consistent spectral shape (Fig. A.3). Fixing the absorption to the values found by XMM gives a consistent black body temperature of kT = 75−115 eV, with a flux reduced by a factor 2–3. The X-ray light curve and spectra of this source are typical for a tidal disruption event, but the optical spectrum shows clear narrow OIII lines, which indicates ongoing AGN activity. It seems very unlikely that a tidal disruption happens within a rare X-ray weak AGN. The temperature of the emission is typical of the effective temperature seen in the ubiquitous soft excess but more interestingly, is also consistent with thermal emission from the inner edge of the accretion disc around a 5×10^5 $M_\odot$ black hole. In this respect the source resembles 2XMM J123103.2+110648 (Terashima et al. 2012; Ho et al. 2012; Lin et al. 2013) and GSN069 (Miniutti et al. 2013), which also host low mass $M \leq 10^6$ $M_\odot$ black holes (see Table 1) and have spectra apparently dominated by thermal emission with little or no contribution from a power law component. The flux detected with the *Swift*-UVOT u filter is constant, within the error range, for observations made between 2006 and 2011.

A.5. XMMSL1 J034555.1-355959

This unclassified AGN at an unknown redshift was detected in a ROSAT pointed observation and later twice in the slew survey. The source was barely detected during the *Swift* follow-up observation, hence no good spectrum is available. The source is variable on relatively short timescales: in 2010 it faded within ten months by a factor of at least eleven.

A.6. XMMSL1 J044347.0+285822

This narrow line Seyfert 1 galaxy is variable because of absorption. Figure A.4 shows the spectra of the three observations made since 2003. The data points of the slew survey correspond to individual photons. However the number of photons at low energies is sufficient to exclude high absorption, while the two later spectra are heavily absorbed.

Ricci et al. (2010) carried out a precise analysis of the XMM pointed observation of 2007 and additional Integral data, where

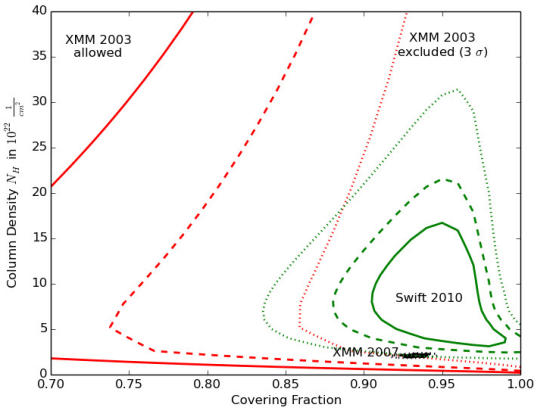

Fig. A.5. The allowed parameter space for one partially covering absorber in the three observations of XMMSL1 J044347.0+285822. Please note that for the slew observation nearly all values except high covering fractions are allowed.

they found two thick partially covering absorbers ($N_{\rm H}$ = 1.4 × 10^{22} cm^{-2} with a covering fraction of 92% and $N_{\rm H}$ = 4 × 10^{22} cm^{-2} with a smaller covering fraction of ∼60%).

To be able to compare this result with the additional less well constrained spectra, we simplify the model using one partially covering absorber only, which still leads to a reasonable fit for the XMM pointed observation. We fix the photon index to 1.5 for all observations, which is the value found in Ricci et al. (2010). In Fig. A.5 we show the allowed parameter space of a partially covering absorber.

While the slew observation excludes high covering fractions and column densities, both the XMM and the *Swift* spectra require them. The best fit of the *Swift* observation is at a higher column density of ∼$N_{\rm H}$ = 1 × 10^{23} cm^{-2} and a slightly higher covering fraction than in the XMM observation. However, at the 3σ level the parameters of these two spectra are compatible, which matches the comparable X-ray fluxes of those two observations. Hence, we conclude that this source is absorbed by a complex structure of neutral hydrogen, which changes with time. It is probable that the observable flux is rather low most of the time, but in the slew observation in 2003 the covering fraction

and/or column density was reduced considerably, such that the AGN appeared brighter by a factor of three to four compared with later observations. It is very likely that the even lower luminosity during the RASS in 1991 was also due to obscuration.

A.7. XMMSL1 J045740.0-503053

For this unclassified galaxy no redshift is known. The source was not seen in the RASS, however in 2002 a bright source was detected in the slew survey. Three years later the source had faded by a factor of at least six and was fainter by a factor 18 in the *Swift* follow-up observation. The *Swift* spectrum has few counts, but can be fitted with an unabsorbed power law with $\Gamma = 1.6 \pm 0.6$.

A.8. XMMSL1 J051935.5-323928

The multi-epoch observations of this Seyfert 1.5 have recently been extensively analysed in (Agís-González et al. 2014) and we perform no further analysis on our *Swift* spectrum here. Agís-González et al. (2014) found that the high-quality spectra were well fit by a disc-reflection model absorbed by a neutral gas column. Strong flux variability was shown to be due to variations in the depth of the absorber which ranged from $N_{\rm H} \sim 5 \times 10^{21}$ cm^{-2} to $N_{\rm H} \sim 3 - 4 \times 10^{23}$ cm^{-2}. Simultaneous variability was seen in the UV confirming the presence of an extended absorber which was identified with the dusty, clumpy torus.

A.9. XMMSL1 J064541.1-590851

The redshift and AGN type are unknown for this source. The XMM slew survey observation in 2006 showed a large flux increase from a RASS upper limit. The *Swift* observation, taken four years later had a similar flux to the slew observation and could be fit with a power law of $\Gamma = 1.9 \pm 0.2$ with no absorption above the Galactic value.

A.10. XMMSL1 J070841.3-493305

This narrow-line Seyfert galaxy is a very well studied source with 1300 ks of total observation time by XMM. Instead of reanalysing the data we summarise the most relevant results here.

The spectra of this AGN have been interpreted as relativistically blurred reflection off an accretion disc around a maximal spinning black hole. Dauser et al. (2012) analyse two XMM spectra from 2008-02-02 and 2010-09-16 during which the source was relatively bright. They find that both spectra are well fit with a steep power law, of photon index ∼2.85, and two reflectors. In addition the fit is improved by adding a mildly relativistic, but highly ionised outflow, which changes its parameters between the two observations.

In January 2011 the source was observed to undergo an extremely X-ray weak phase, a factor 190 below the highest observed flux in the soft X-ray band. An XMM spectrum taken on 2011-01-12 had a soft-band flux a factor of ten lower than the combined spectra from the year 2008. However, in the hard band, which is dominated by the Fe line, a change by a factor of just two is observed. Fabian et al. (2012) analysed those spectra in detail finding that by 2011 the power law emission had disappeared. By examining the relativistically broadened Fe Kα line, they are able to constrain the part of the disc at which the X-rays are scattered. While in 2008 around 50% of the X-ray flux came from within the inner disc, within one gravitational radius of the event horizon, 90% of the radiation came from this part of the disc in the January 2011 observation. They interpret this as the corona collapsing to a compact source very close to the black hole. Due to light-bending effects very few X-rays can escape and contribute to the power law continuum, while most of them are focussed on the disc, which increases the reflection features.

Even though this is an explanation of the temporary low luminosity state at the beginning of 2011, it is not clear whether the same mechanism is responsible for the large amplitude variability observed over a period of more than a decade.

The relative X-ray luminosity of this source is by far the lowest, at $\alpha_{\rm OX} = -2.5$. It deviates by more than a factor of 700 from the expected value. Since none of the other sources get close to this value, we conclude that this source is exceptional even in this sample of highly variable AGN.

A.11. XMMSL1 J082753.7+521800

This source is a bright radio loud quasar at redshift 0.33 and a luminous infrared galaxy. The X-ray spectrum is well described by a simple power law, but a highly ionised absorber can not be ruled out and could cause a flux change by up to a factor of three. The source is radio loud and thus jet activity might be a more likely explanation of the observed variability.

A.12. XMMSL1 J090421.2+170927

This broad-line QSO at a redshift of 0.073 was not detected during the RASS or in two further ROSAT pointed observations. The detection in the slew survey is brighter by a factor of 28 compared to the lowest upper limit. Four years later in the *Swift* follow-up observation the source had faded by a factor of three to four. The spectrum is rather flat. When fitted with a single power law, the photon index is as low as $\Gamma = 0.9 \pm 0.5$. If the photon index is fixed to 1.7 and an ionised absorber added, the fitted column density of $(1.6^{+4.3}_{-1.6}) \times 10^{21}$ cm^{-2} can explain a flux change sufficient to explain the brightest observation in the slew survey. However, the spectrum has too few counts to verify that an absorber is present. We conclude therefore that variability due to absorption is a possible scenario for this source.

A.13. XMMSL1 J093922.5+370945

The spectrum and flux of XMMSL1 J093922.5+370945 varied little between an XMM pointed observation of 2006 and *Swift* observations of 2007 and 2011 and can be well fitted with a single power law ($\Gamma \sim 3$) with no evidence of intrinsic absorption (Fig. A.6). The steep power-law slope is typical of a narrow-line Seyfert 1 galaxy (Esquej et al. 2007). The variability mechanism is unknown, although a reasonable assumption would be that it shares the same mechanism as the other NLS1 in our sample, XMMSL1 J070841.3-493305.

A.14. XMMSL1 J100534.8+392856

The slew survey and *Swift* observations of this galaxy show a similar flux, a factor of between nine and fifteen above the RASS upper limit. The *Swift* spectra may both be fitted with an unabsorbed power law and a common power law index of $\Gamma = 1.9 \pm 0.2$. The narrow [OIII]λ5007 line in the optical spectrum is relatively weak, $L_{\rm X}/L_{\rm [OIII]} \sim 1000$ well in excess of the ratio

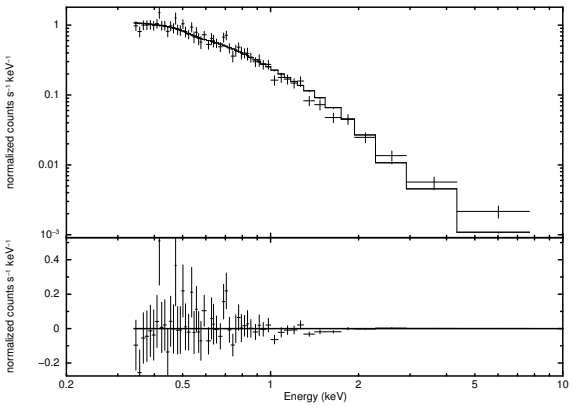

Fig. A.6. A power-law fit to the XMM pointed observation spectrum of XMMSL1 J093922.5+370945 from 2006-11-01. The spectrum is soft with $\Gamma \sim 3$.

of 1−100 usually seen in Seyfert galaxies (Panessa et al. 2006). As $L_{[OIII]}$ represents a measure of the integrated historical bolometric luminosity this suggests that the intrinsic emission is currently at a high level.

A.15. XMMSL1 J104745.6-375932

This AGN showed a clear Sy 1 profile at a redshift of 0.075, in the 6dF survey of the Anglo-Australian Telescope (AAT). It was not detected in the RASS but has been seen three times since 2003. The last, and faintest, detection with *Swift* revealed a power law spectrum of photon index $\Gamma = 2 \pm 0.2$ with no additional absorption above the Galactic column.

A.16. XMMSL1 J111527.3+180638

This source has been reported as a low-redshift, candidate tidal disruption event by Esquej et al. (2007, 2008).

A.17. XMMSL1 J112841.5+575017

This Seyfert 2 was not detected during the RASS, but was found to be bright during the slew survey and *Swift* follow-up observations. The spectrum in 2013 may be fitted adequately with a pure power law model ($\Gamma = 1.7 \pm 0.1$). Since the only available spectrum corresponds to the brightest state we cannot exclude a varying column density of the absorber as a variability mechanism. In the brightest observation the X-ray luminosity nearly matches the one expected from the UV flux while the ROSAT upper limit is X-ray weak.

A.18. XMMSL1 J113001.8+020007

This is most likely to be a spurious detection. It was only detected in one XMM slew observation and the counterpart is a rather faint, $g = 21.4$ galaxy, SDSS J113001.72+015956.6. The significance of the slew detection is rather high, but a visual inspection shows that the photons lie in a line rather than coming from an obvious point source.

A.19. XMMSL1 J121335.0+325609

This broad-line QSO at a redshift of $z = 0.222$ has been observed to be variable for over 30 years. Nevertheless, due to the short exposure times no good spectrum is available. The source was detected twice by ROSAT, the first time at an intermediate level, and shortly afterwards at its currently lowest observed state, a factor of more than 20 dimmer. Since 2006 the source has been detected five times by *Swift* and during the slew survey. In those observations the source was found to have a bright or intermediate luminosity and a change by a factor of seven has been observed within 17 months. The UVOT flux was constant during the *Swift* observations. However in an additional short observation, nine months after the last X-ray data the UV flux had increased by 30%. The merged spectrum of the three *Swift* observations in 2006 with a flux five times below the slew detection may not be explained by a thick absorber and the variability mechanism remains unclear.

A.20. XMMSL1 J132342.3+482701

The variability in this non-active galaxy has been interpreted as a tidal disruption event (see Esquej et al. 2007, 2008 for details).

A.21. XMMSL1 J162553.4+562735

This QSO, at redshift 0.3, was not seen in the RASS but has been detected in all observations since 2005 with a slowly decreasing luminosity. The 2010-07-10 *Swift* spectrum has few counts and can be described by a pure power law with $\Gamma = 2.3 \pm 0.5$ (see Table B.1). A significant absorption column can be excluded. While the slew observation matches the expected X-ray to UV ratio, the ROSAT upper limit corresponds to a rather X-ray weak state. The quasar is bright in the infrared and can be classified as a LIRG.

A.22. XMMSL1 J173738.2-595625

This is the Seyfert 2 galaxy, ESO 139-G12 which has been mooted as a possible site of cosmic-ray acceleration (Terrano et al. 2012). It was observed eight times by *Swift* in 2008 and 2013, where it varied by a factor five. The *Swift* spectra can be fitted simultaneously with a power law of slope $\Gamma = 1.90 \pm 0.04$ of variable normalisation, absorbed by the Galactic column (Fig. A.7; C/d.o.f. = C_{red} = 1565/1641). There is no obvious evidence for intrinsic absorption in the spectra. A small improvement in the fit can be achieved by adding a soft-excess component, represented by a black body ($kT = 151 \pm 28$ eV; C_{red} = 1535/1633). To check whether the dip on 2008-06-03 is due to absorption we fit this spectrum simultaneously with the brighter spectrum from 2008-05-04. A power law ($\Gamma = 1.96 \pm 0.10$) with variable normalisation and Galactic absorption gives a good fit (C_{red} = 344/375). Fixing the normalisation between the two spectra and adding a cold (warm) absorption component to the 2008-06-03 spectrum gives a poor fit of C_{red} = 517/375 (431/374). Allowing the normalisation to vary and adding a warm absorber to the fainter spectrum gives no improvement (C_{red} = 344/373). Therefore the variability in this source is likely to be intrinsic. The relative X-ray luminosity is, however, somewhat low in this source, even in the brightest state (see Table 2) and so another possibility is that variability is due to partial covering of the central source by a compton-thick absorber.

A.23. XMMSL1 J183521.4+611942

This flat-spectrum radio quasar, at a redshift of 2.2, is the most distant and luminous object in our sample, with a peak

luminosity of $L_X \sim 6 \times 10^{46}$ erg s^{-1} and $M_{BH} = 10^{9.7}$ $M_\odot$ derived from the k-band luminosity. The low count X-ray spectrum is not well fit by a simple power law but an absorber does not improve the fit. Therefore, variable jet activity is perhaps the most likely cause.

A.24. XMMSL1 J193439.3+490922

This unclassified galaxy with an unknown redshift was detected three times in the slew survey from 2003 to 2006 but was not seen in the RASS nor during the *Swift* follow-up observation. By combining the 20 photons available from the three slew survey detections we can make a crude spectrum. A fit to this gives a typical AGN-like power law slope of $\Gamma = 2.1 \pm 0.5$.

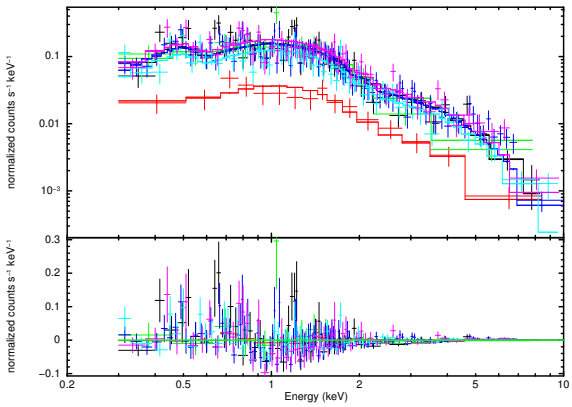

Fig. A.7. Simultaneous fit to eight *Swift* spectra from XMMSL1 J173738.2-595625 of a power law, of fitted index $\Gamma = 1.90 \pm 0.04$, absorbed by the Galactic column. The normalisation is fairly constant, only varying significantly for the spectrum from 2008-06-03 (red), where it is lower than the brightest spectrum by a factor of five. This change in flux rate is reflected as a dip in the X-ray light curve (see Fig. B.1v). Additional absorption is not required to fit the spectra

.

Table A.1. Observations used in this study.

XMMSL1 name	Instrument	ObsID	Date[a]	$T_{\rm exp}$ (s)[b]
J005953.1+314934	Einstein MPC	2619	1980-01-10	2211
	ROSAT	RASS	1991-01-01	462
	ROSAT PSPC	WG701087P.N1	1992-07-18	4292.8
	XMMSL1	9038500002	2002-01-15	8.8
	XMM EPIC pn	0312190101	2006-01-24	11193
	Swift XRT	00035243	2006-05-29 – 2006-05-31	31181
	Suzaku	704025010	2010-01-06 – 2010-01-07	91000
	Swift XRT	00040300*	2011-02-07 – 2011-08-29	3444
J015510.9-140028	ROSAT PSPC	RASS	1991-01-01	468
	ROSAT PSPC	rp600005n00	1992-01-15	15850
	XMMSL1	9075100004	2004-01-15	6.0
	Swift XRT	00040302*	2010-06-06 – 2010-09-14	1610
J020303.1-074154	ROSAT	RASS	1991-01-01	400
	XMMSL1	9075000006	2004-01-14	4.7
	XMM EPIC pn	0411980201	2006-07-03	10828
	Swift XRT	00035746001	2007-06-03	3270
	Swift XRT	00035746002	2008-03-02	3668
	Swift XRT	00040304001*	2010-03-01	2422
J024916.6-041244	ROSAT PSPC	RASS	1991-01-01	238
	XMMSL1	9084700002	2004-07-25	1.90
	XMM EPIC pn	0411980401	2006-07-14	9865
	Swift XRT	00035748002,3	2006-12-06 – 2006-12-07	959
	Swift XRT	00035748004	2007-01-26	649
	Swift XRT	00035748005	2007-06-27	3054
	Swift XRT	00040306001,2,3*	2010-06-13 – 2011-03-08	2145
	Swift XRT	00040306004,5*	2015-03-03 – 2015-03-06	2812
J034555.1-355959	ROSAT	RASS	1991-01-01	70
	ROSAT PSPC	rp800300n00	1992-08-27	1217
	ROSAT PSPC	rp800300a01	1993-01-26	3600
	ROSAT PSPC	rp190499n00	1997-02-06	2005
	XMMSL1	9156600004	2008-06-28	6.4
	XMMSL1	9186200002	2010-02-07	5.2
	Swift XRT	00040307001*	2010-12-22 – 2010-12-23	2361
J044347.0+285822	ROSAT	RASS	1991-01-01	454
	XMMSL1	9058800004	2003-02-24	3.8
	XMM EPIC pn	0401790101	2007-03-18	10042
	Swift XRT	00040308001*	2010-07-27	1806
J045740.0-503053	ROSAT	RASS	1991-01-01	400
	XMMSL1	9049100003	2002-08-14	4.5
	XMMSL1	9102600004	2005-07-16	8.3
	XMMSL1	9188000003	2010-03-16	8.3
	Swift XRT	00040309001*	2010-11-06	2284
	Swift XRT	00040309002,3,5*	2013-04-05 – 2013-05-11	5100
J051935.5-323928[c]	ROSAT	RASS	1991-01-01	505
	Swift campaign	35234	2005-10-29 – 2005-11-26	
	XMMSL1	0312190701	2006-01-28	8726
	XMMSL1	9124900007	2006-10-05	6.4
	Suzaku	703014010	2008-04-11	83410
	XMMSL1	9179700004	2009-10-01	5.66
	XMMSL1	9196400008	2010-08-31	7.41
	Swift campaign	31868	2010-11-15 – 2011-01-21	
	Swift XRT	00040311001,2*	2011-01-07 – 2011-01-23	2309

Notes. *Swift* observations taken specifically for this programme are marked with *. [(a)] For the ROSAT all-sky survey, 1991-01-01 is assumed as an approximate observation date for all observations. [(b)] The exposure time for the *XMM-Newton* slew observations is given for the total energy band. There is a small difference, due to the energy-dependent vignetting, when considering the soft or hard band only. [(c)] Numerous observations from other campaigns are available, many are shown in the light curve. Here we only list ROSAT, XMM and our *Swift* observations. [(d)] In addition there are *Chandra* observations which are not considered here.

Table A.1. continued.

XMMSL1 name	Instrument	ObsID	Date[a]	T_{exp} (s)[b]
J064541.1-590851	ROSAT	RASS	1991-01-01	645
	XMMSL1	9126300002	2006-11-01	3.5
	XMMSL1	9143600003	2007-10-13	6.2
	XMMSL1	9159400002	2008-08-22	8.4
	XMMSL1	9195100003	2010-08-04	7.3
	Swift XRT	00040315001,2*	2010-12-22 – 2010-12-26	2455
	XMMSL1	9241500003	2013-02-15	1.0
	XMMSL1	9255200003	2013-11-15	6.1
J070841.3-493305[c]	ROSAT	RASS	1991-01-01	171
	ROSAT	rp180306n00	1998-12-09	9472
	XMM EPIC pn	0110890201	2000-10-21	40700
	XMM EPIC pn	0148010301	2002-10-13	78000
	XMMSL1	9109200003	2005-11-25	2.9
	XMM campaign	0506200201-501	2007-05-16 – 2007-07-06	
	XMMSL1	9143400002	2007-10-09	9.3
	XMM campaign	0511580101-1201	2008-01-29 – 2008-02-06	
	XMM campaign	0653510301-601	2010-09-13 – 2010-09-19	
	Swift campaign	90393	2010-04-03 – 2010-12-19	
	Swift XRT	00040317001*	2010-12-22	1569
	XMM EPIC pn	0554760801	2011-01-12	96000
	Swift campaign	90393	2010-12-23 – 2011-01-25	
	Swift XRT	00040317003*	2011-01-27	476
	Swift campaign	90393	2011-01-28 – 2011-03-29	
	XMMSL1	9207000003	2011-03-30	6.9
	Swift campaign	91623	2013-05-20 – 2013-06-19	
	Swift campaign	80720	2014-05-05 – 2014-06-28	
J082753.7+521800	ROSAT	RASS	1991-01-01	449
	XMMSL1	9106500003	2005-10-02	8.4
	Swift XRT	00040320001*	2010-03-11	2159
J090421.2+170927	ROSAT	RASS	1991-01-01	310
	ROSAT PSPC	rs931424n00	1991-11-18	4170
	XMMSL1	9126300002	2006-11-01	4.6
	Swift XRT	00040322001*	2010-06-12	1794
J093922.5+370945	ROSAT	RASS	1991-01-01	470
	XMMSL1	9081300003	2004-05-18	7.7
	XMM Epic pn	0411980301	2006-11-01	5038
	Swift XRT	00035747001	2007-09-21	6554
	Swift XRT	00040325001,2*	2011-03-28 – 2011-05-11	1846
J100534.8+392856	ROSAT	RASS	1991-01-01	481
	XMMSL1	9107400003	2005-10-21	1.0
	Swift XRT	00040326001*	2011-01-31	2058
	Swift XRT	00040326004*	2013-04-23	3654
J104745.6-375932	ROSAT	RASS	1991-01-01	362
	XMMSL1	9073500003	2003-12-14	7.6
	XMMSL1	9173700002	2009-06-03	9.1
	Swift XRT	00040328001,2*	2010-04-11 – 2010-04-16	2288
J111527.3+180638[d]	ROSAT	RASS	1991-01-01	383
	XMMSL1	9072400006	2003-11-22	8.0
	XMM EPIC pn	0411980101	2006-06-23	5017
	Swift XRT	00035745001	2006-12-01	5773
	XMM EPIC pn	0556090101	2008-12-02	41734
	Swift XRT	00040332001,2*	2010-10-23 – 2010-11-16	2614
	Swift XRT	00084368001,2	2014-07-17 – 2014-10-23	5936
J112841.5+575017	ROSAT	RASS	1991-01-01	519
	XMMSL1	9107500006	2005-10-23	10.5
	XMMSL1	9116700004	2006-04-24	5.5
	Swift XRT	00040333001*	2011-03-28	1872
	Swift XRT	00040333002,3,4*	2013-04-10 – 2013-10-19	6196
J113001.8+020007	ROSAT	RASS	1991-01-01	427
	XMMSL1	9109400004	2005-11-29	6.7
	XMMSL1	9165400002	2008-12-20	4.6
	XMMSL1	9183300003	2009-12-13	5.9
	Swift XRT	00040334001,2*	2011-01-26 – 2011-01-31	2041

Table A.1. continued.

XMMSL1 name	Instrument	ObsID	Date[a]	T_{exp} (s)[b]
J121335.0+325609	ROSAT	RASS	1991-01-01	502
	ROSAT	rp600130n00	1991-11-24	16310
	XMMSL1	9072500005	2003-11-24	9.0
	Swift campaign	55300	2006-06-02	2910
	Swift campaign	55300	2006-06-09 – 2006-06-12	4369
	Swift campaign	55300	2006-06-27	1814
	XMMSL1	9155100004	2008-05-29	10.1
	Swift XRT	00040335001*	2010-10-19	1589
	Swift XRT	00040335002*	2011-07-06	398
J132342.3+482701	ROSAT	RASS	1991-01-01	560
	XMMSL1	9072900002	2003-12-01	8.6
	XMM EPIC pn	0411980501	2006-07-15	5018
	Swift XRT	00035749001	2007-01-11	3854
	Swift XRT	00035749002	2007-05-26	1922
	Swift XRT	00040336001*	2011-02-04	1819
J162553.4+562735	ROSAT	RASS	1991-01-01	1035
	XMMSL1	9100800002	2005-06-10	5.8
	XMMSL1	9131700004	2007-02-17	4.0
	Swift XRT	00040345001,2*	2010-07-10 – 2010-07-11	3753
	Swift XRT	00040345004,5*	2013-04-08 – 2013-04-14	3987
J173739.3-595625[d]	ROSAT	RASS	1991-01-01	165
	XMMSL1	9123400007	2006-09-05	2.9
	XMMSL1	9151100003	2008-03-10	5.5
	Swift XRT	00037391001	2008-05-04	1958
	Swift XRT	00037705001	2008-06-03	2671
	Swift XRT	00037705002	2008-07-10	553
	Swift XRT	00037391002	2008-07-21	5001
	Swift XRT	00037391003	2008-07-29	3359
	Swift XRT	00037705004	2008-11-02	2078
	Swift XRT	00040349001*	2013-03-18	125
	Swift XRT	00040349002,3*	2013-10-12 – 2013-10-18	1747
J183521.4+611942	ROSAT	RASS	1991-01-01	2270
	XMMSL1	9100300002	2005-05-31	1.0
	XMMSL1	9149600002	2008-02-09	8.4
	XMMSL1	9173900002	2009-06-08	10.1
	Swift XRT	00040352001*	2011-02-04	1914
	Swift XRT	00040352003,4,5,6*	2013-06-16 – 2013-07-24	2970
J193439.3+490922	ROSAT	RASS	1991-01-01	823
	XMMSL1	9072800002	2003-11-30	9.2
	XMMSL1	9100700002	2005-06-08	8.2
	XMMSL1	9127200003	2006-11-19	4.8
	Swift XRT	00040353002,3,4,5*	2011-11-24 – 2012-09-15	2237

Table A.2. Summary of proposed variability mechanism.

XMMSL1 name	Type	z	Variability causes and comments
Sources displaying factor >10 variability between ROSAT and XMM, and XMM and *Swift* epochs			
J015510.9-140028	–	–	spurious slew detection
J024916.6-041244	Sy 1.9	0.0186	soft, absorbed black body spectrum; variability likely intrinsic in nature due to constant spectral shape
J034555.1-355959	–	–	inconclusive
J045740.0-503053	–	–	inconclusive
J051935.5-323928	Sy 1.5	0.0125	other studies suggest variable absorption
J070841.3-493305	NLS 1	0.0406	intrinsic power law changes; studies suggest variable reflection off disc
J111527.3+180638	liner	0.00278	tidal disruption event
J113001.8+020007	–	–	spurious slew detection
J132342.3+482701	non-active	0.0875	tidal disruption event
J193439.3+490922	–	–	unclear; only detected during three XMM slews
Sources displaying factor >10 variability between ROSAT and XMM epochs			
J005953.1+314934	Sy 1.2	0.0149	neutral and ionised partially covering absorbers
J020303.1-074154	Sy 1	0.0615	spectral shape unaltered since 2004 indicating intrinsic flux change; little variability since 2006
J044347.0+285822	Sy 1	0.0217	neutral partial covering absorbers
J064541.1-590851	–	–	inconclusive; no evidence for significant variability since 2006; bright state spectra do not require absorption
J082753.7+521800	QSO, RL	0.3378	no absorption required in bright state, likely jet variability
J090421.2+170927	QSO	0.0733	possibly ionised absorption
J093922.5+370945	NLS 1	0.1861	inconclusive; bright state spectra do not require absorption
J100534.8+392856	Sy 1	0.1409	bright state spectrum does not require absorption; possibly increased intrinsic emission.
J104745.6-375932	Sy 1	0.0755	absorption-only excluded; faintest state does not require absorption
J112841.5+575017	Sy 2	0.0509	inconclusive; brightest state does not require absorption
J121335.0+325609	QSO	0.222	inconclusive
J162553.4+562735	QSO	0.307	soft spectrum; absorption-only excluded
J173739.3-595625	Sy 2	0.0170	intrinsic; constant spectral shape from 2008–2013
J183521.4+611942	blazar, RL	2.274	inconclusive; likely jet contribution

Appendix B: Additional material

Table B.1. Best fitting models for all spectra analysed here.

XMMSL1 name	Obs. date	Instr.	$C_{\rm red}$	Power law Γ	Cold abs. $N_{\rm H}$ (10^{22} cm^{-2})	Warm abs. $N_{\rm H}$ (10^{22} cm^{-2})	log(ξ)
J005953.1+314934	2002-01-15	XMMSL	1.01	2.21 (F)	–	–	–
	2006-01-24	XMM P.	0.95	$2.21^{+0.08}_{-0.10}$	$2.3^{+0.4}_{-0.5}$, $f_{\rm c} = 0.36^{+0.08}_{-0.10}$	117^{+44}_{-62}, $f_{\rm c} = 0.81^{+0.07}_{-0.17}$	$2.05^{+0.12}_{-0.06}$
	2006-05-29	*Swift*	1.04	2.21 (F)	2.3 (F), $f_{\rm c} = 0.50 \pm 0.03$	–	–
	2011-08-28	*Swift*	0.79	2.21 (F)	2.3 (F), $f_{\rm c} < 0.28$	–	–
J020303.1-074154	2006-07-03	XMM P.	0.95	$2.31^{+0.07}_{-0.06}$	–	$2.6^{+1.1}_{-0.5}$	$1.94^{+0.17}_{-0.06}$
	2007-06-03	*Swift*	0.77	2.2 ± 0.2	–	–	–
	2008-03-02	*Swift*	1.06	1.9 ± 0.2	–	–	–
	2010-03-01	*Swift*	0.88	1.5 ± 0.4	–	–	–
J024916.6-041244	2006-07-14	XMM P.	1.11	$kT = 124^{+17}_{-12}$ eV	$0.14^{+0.02}_{-0.03}$	65^{+11}_{-5}	$2.95^{+0.03}_{-0.05}$
	2007-07-14	*Swift*	0.55	$kT = 100^{+24}_{-21}$ eV	0.14 (F)	65 (F)	2.95 (F)
J044347.0+285822	2007-03-18	XMM P.	1.00	1.59 ± 0.12	$1.3^{+0.3}_{-0.4}$, $f_{\rm c} = 0.92^{+0.02}_{-0.04}$ $4.3^{+1.6}_{-1.2}$, $f_{\rm c} = 0.64 \pm 0.11$	-	-
	2010-07-27	*Swift*	1.06	1.59 (F)	10^{+8}_{-4}, $f_{\rm c} = 0.95^{+0.03}_{-0.04}$	–	–
J045740.0-503053	2010-10-03	*Swift*	0.99	1.6 ± 0.6	–	–	–
J064541.1-590851	2010-12-26	*Swift*	0.75	1.9 ± 0.2	–	–	–
J082753.7+521800	2010-03-11	*Swift*	1.11	2.0 ± 0.3	–	–	–
J090421.2+170927	2010-06-12	*Swift*	0.86	1.7 (F)	–	$3.0^{+4.6}_{-2.3}$	$1.38^{+0.68}_{-0.88}$
J093922.5+370945	2006-11-01	XMM P.	1.07	2.94 ± 0.07	–	–	–
	2007-09-21	*Swift*	0.68	2.7 ± 0.3	–	–	
	2011-03-28	*Swift*	1.15	3.0 ± 0.4	–	–	
J100534.8+392856	2011-01-31	*Swift*	1.20	1.9 ± 0.2	–	–	–
	2013-04-23	*Swift*	0.81	1.75 ± 0.15	–	–	–
J104745.6-375932	2010-04-11	*Swift*	0.89	2.0 ± 0.2	–	–	–
J112841.5+575017	2013-04-10	*Swift*	0.82	1.7 ± 0.1	–	–	–
J121335.0+325609	2010-10-19	*Swift*	1.03	2.1 ± 0.4	–	–	–
J162553.4+562735	2010-07-10	*Swift*	0.87	2.3 ± 0.5	–	–	–
J173739.3-595625	2008-05 – 2008-11	*Swift*	1.03	1.85 ± 0.07	–	–	–
J183521.4+611942	2011-02-04	*Swift*	1.49	1.9 ± 0.5	–	–	–

Notes. XMMSL = slew survey observation, XMM P. = pointed XMM observation. Galactic absorption was included and fixed in all fits. Parameters followed by "(F)" were frozen. XMMSL1 J005953.1+314934 was fit with an absorbed power law plus black body model, J024916.6-041244 was fitted with an absorbed black body spectrum only, J044347.0+285822 has two partially-covering neutral absorbers in the 2007 observation. $f_{\rm c}$ is the covering fraction of the absorber. Errors are quoted at 90% confidence.

Table B.2. Allowed column densities of neutral hydrogen.

XMMSL1 name	Obs. date	$C_{\rm red}$	Spectral index	$N_{\rm H,\,max}$[a] (10^{20} cm^{-2})	Implied[b] flux change	Observed[c] flux change	Can it explain variability?
J005953.1+314934	2011-08-28	0.87	1.9	1.6	1.1	1.9	no
J020303.1-074154	2010-03-01	0.90	1.7[d]	1.3	1.2	5.8	no
J024916.6-041244	2007-06-27	0.95	1.7[d]	2.3	1.2	17	no
J044347.0+285822	2010-07-27	1.07	1.7[d]	554	117	7.3	yes
J045740.0-503053	2010-10-03	1.00	1.7[d]	16.9	2.0	17	no
J064541.1-590851	2010-12-26	0.77	1.9	5.58	1.2	1.4	maybe
J082753.7+521800	2010-03-11	1.12	2.0	4.76	1.2	2.7	no
J090421.2+170927	2010-06-12	1.21	1.7[d]	75	2.7	3.6	no
J093922.5+370945	2011-03-28	1.17	3.0	12.8	2.5	3.4	no
J100534.8+392856	2011-01-01	1.22	1.9	1.55	1.1	1.7	no
J104745.6-375932	2010-04-11	0.90	2.0	2.97	1.2	1.6	no
J112841.5+575017	2011-03-01	0.86	1.7[d]	7.20	1.5	–	*Swift* point brightest
J121335.0+325609	2006-06[e]	0.97	1.4	6.6	1.3	4.9	no
J162553.4+562735	2010-07-10	0.88	2.3	10.2	1.6	3.2	no
J173739.3-595625	2008-11-02	0.91	1.9	1.4	1.1	2.0	no
J183521.4+611942	2011-02-01	1.51	1.7[d]	16.2	1.4	5.4	no

Notes. [(a)] Maximum neutral Hydrogen column allowed by power law fit to the *Swift* spectrum (90% confidence). [(b)] Fractional change in observed 0.2–2 keV flux due to this $N_{\rm H}$ column. [(c)] Change in 0.2–2 keV flux actually observed between the highest flux measurement and the *Swift* observation. [(d)] Power law slope fixed at 1.7 during fit. [(e)] Merged spectra taken between 2006-06-02 and 2006-06-12.

Table B.3. Allowed column densities of ionised gas.

XMMSL1 name	Obs. date	$C_{\rm red}$	Spectral index	Ionisation[a]	$N_{\rm H,\,max}$[b] (10^{20} cm^{-2})	Implied[c] flux change	Observed[d] flux change	Can it explain variability?
J005953.1+314934	2011-08-28	1.07	1.7[e]	low	5.1	1.2	1.9	no
J020303.1-074154	2010-03-01	0.74	1.7[e]	high	69	3.3	5.8	no
J024916.6-041244	2007-06-27	1.03	1.7[e]	high[f]	150	110	17	yes
J044347.0+285822	2010-07-27	1.05	1.7[e]	low	210	260	7.3	yes
J045740.0-503053	2010-10-03	0.99	1.7[e]	medium	72	2.5	17	no
J064541.1-590851	2010-12-26	0.77	2.0	high	190	1.6	1.4	yes
J082753.7+521800	2010-03-11	1.13	2.3	high	650	3.2	2.7	yes
J090421.2+170927	2010-06-12	0.83	1.7[e]	high	1400	7.3	3.6	yes
J093922.5+370945	2011-03-28	1.20	3.2	low	9.9	2.2	3.4	no
J100534.8+392856	2011-01-01	1.22	1.7[e]	high	180	1.5	1.7	maybe
J104745.6-375932	2010-04-11	0.88	2.2	high	700	1.7	1.6	yes
J112841.5+575017	2011-03-01	0.74	1.7[e]	high	7.0	3.1	–	*Swift* point brightest
J121335.0+325609	2006-06[g]	0.99	1.5	low	7.9	1.3	4.9	no
J162553.4+562735	2010-07-10	0.89	2.2	low	13	1.9	3.2	no
J173739.3-595625	2008-11-02	0.91	2.0	high	140	1.4	2.0	no
J183521.4+611942	2011-02-01	1.51	1.7[e]	high	610	1.6	5.4	no

Notes. [(a)] Ionisation level which yields largest flux change: low ($\log(\xi) = -1$); medium ($\log(\xi) = 0.5$); high ($\log(\xi) = 2$). [(b)] Maximum ionised hydrogen column allowed by power law fit to the *Swift* spectrum (90% confidence). [(c)] Fractional change in observed 0.2–2 keV flux due to this $N_{\rm H}$ column. [(d)] Change in 0.2–2 keV flux actually observed between the highest flux measurement and the *Swift* observation. [(e)] Power law slope fixed at 1.7 during fit. [(f)] A medium ionisation level yields even stronger absorption, however the fit is worse. [(g)] Merged spectra taken between 2006-06-02 and 2006-06-12.

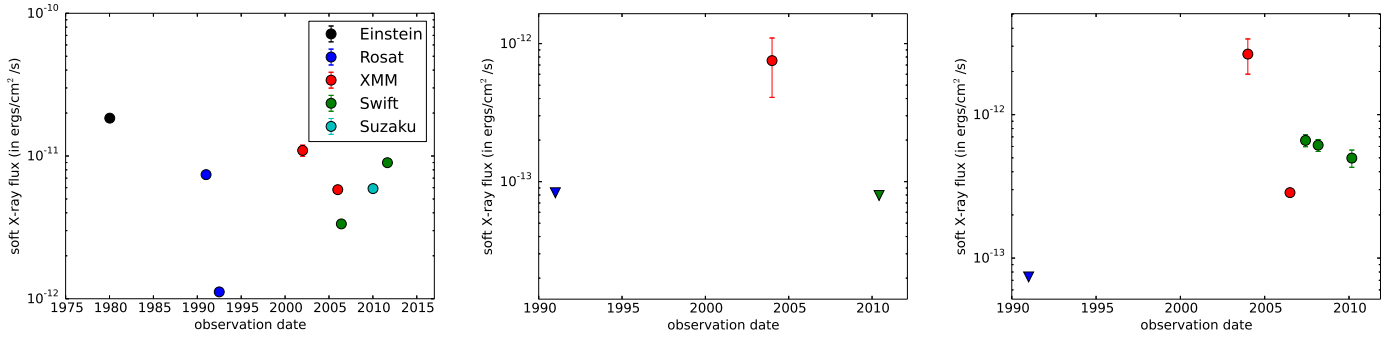

(a) XMMSL1 J005953.1+314934 (b) XMMSL1 J015510.9-140028 (c) XMMSL1 J020303.1-074154

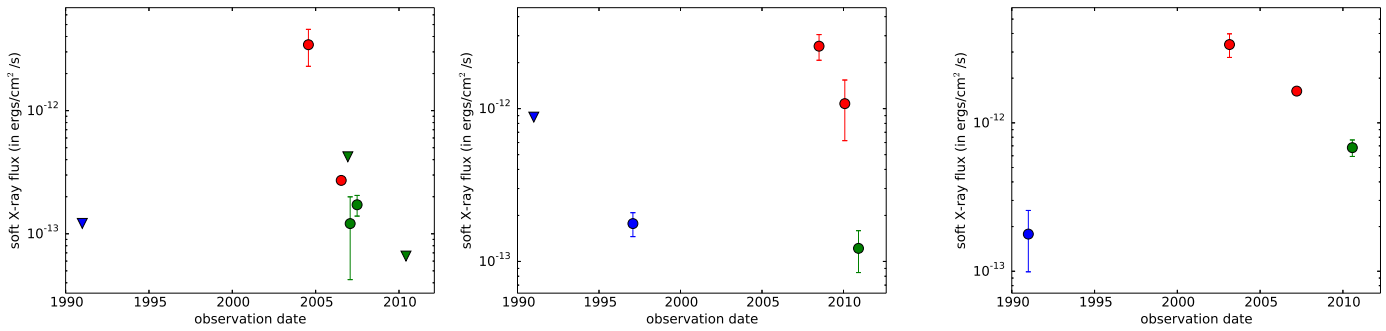

(d) XMMSL1 J024916.6-041244 (e) XMMSL1 J034555.1-355959 (f) XMMSL1 J044347.0+285822

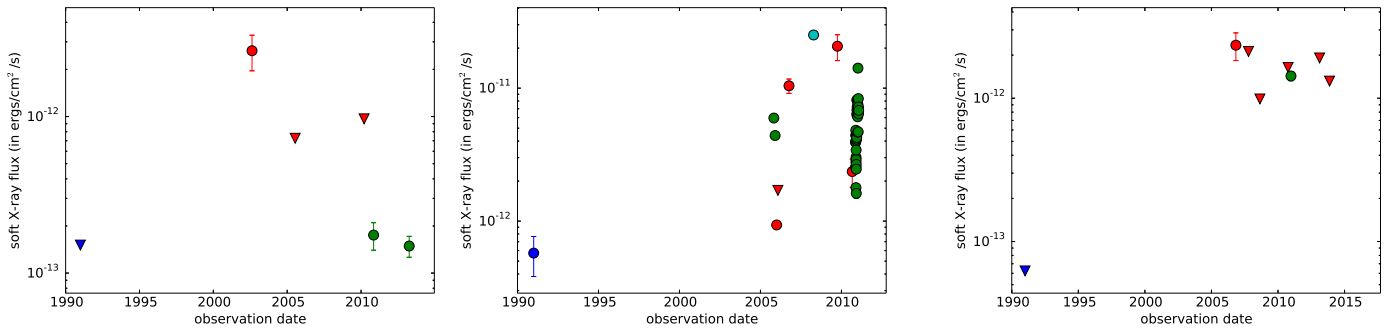

(g) XMMSL1 J045740.0-503053 (h) XMMSL1 J051935.5-323928 (i) XMMSL1 J064541.1-590851

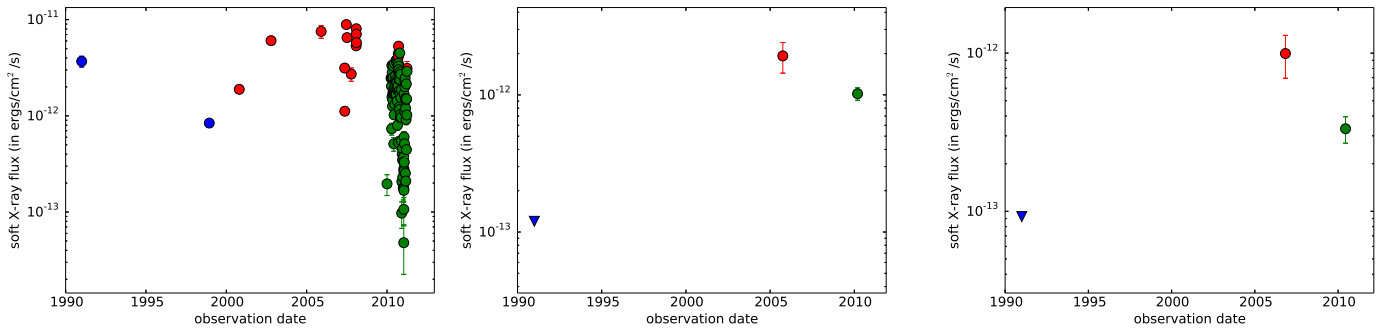

(j) XMMSL1 J070841.3-493305 (k) XMMSL1 J082753.7+521800 (l) XMMSL1 J090421.2+170927

Fig. B.1. Soft X-ray (0.2–2 keV) light curves for all the sources in our sample. Count rates of the different telescopes were converted to the 0.2–2.0 keV range using PIMMS under the assumption that the spectral shape can be described by a power law with a photon index of 1.7 and absorption in our Galaxy alone. Circles represent detections, while triangles symbolise 95% upper limits on the flux. All error bars are 1σ.

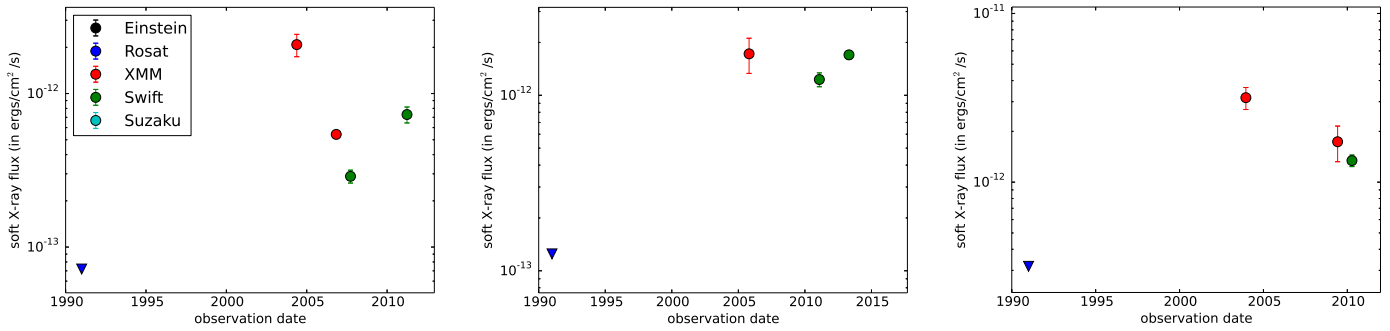

(m) XMMSL1 J093922.5+370945 (n) XMMSL1 J100534.8+392856 (o) XMMSL1 J104745.6-375932

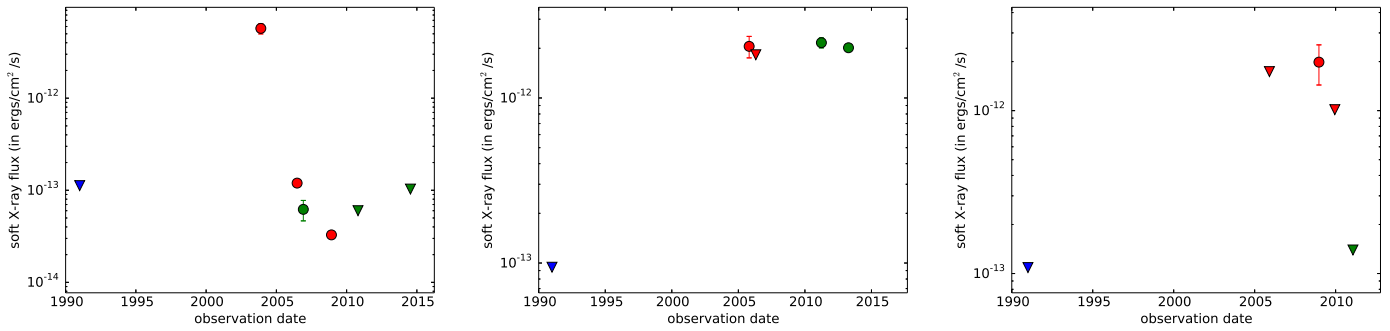

(p) XMMSL1 J111527.3+180638 (q) XMMSL1 J112841.5+575017 (r) XMMSL1 J113001.8+020007

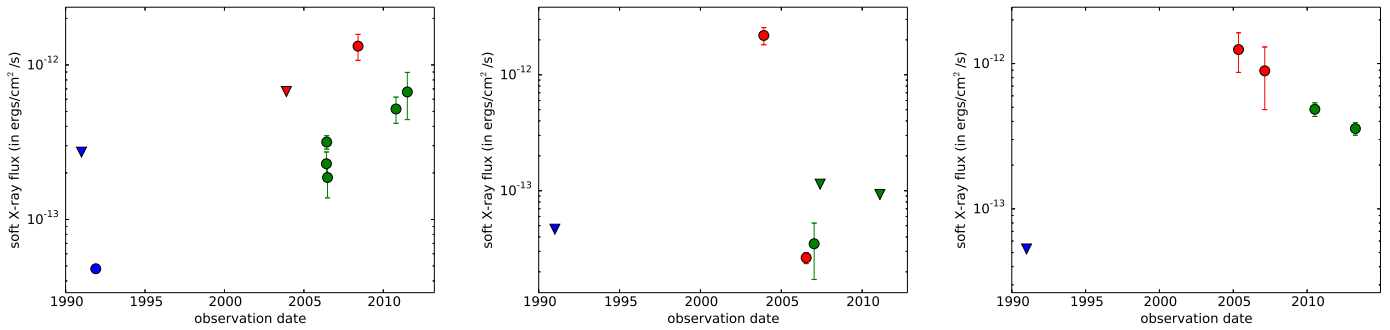

(s) XMMSL1 J121335.0+325609 (t) XMMSL1 J132342.3+482701 (u) XMMSL1 J162553.4+562735

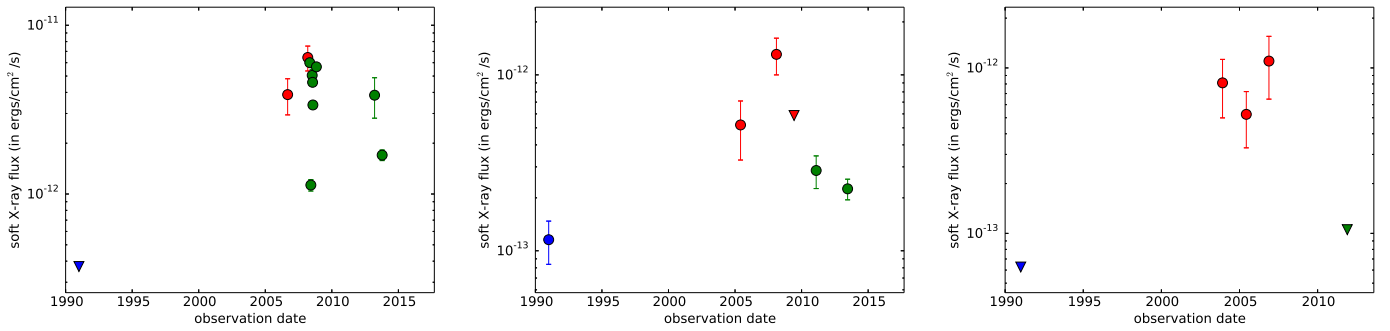

(v) XMMSL1 J173738.2-595625 (w) XMMSL1 J183521.4+611942 (x) XMMSL1 J193439.3+490922

Fig. B.1. continued.